Chapter 1

Introduction

1.1 Nuclear Spin Relaxation

Many atomic nuclei have a non-zero spin angular momentum in their ground state, and as such have a magnetic dipole moment. Different orientations of the magnetic moments with respect to an applied magnetic field B_0 correspond to different magnetic energies E_m. According to the Boltzmann law, the populations P_m of the energy levels are therefore proportional to $\exp(-E_m/kT)$, where k is the Boltzmann constant and T is the absolute temperature. A sample containing N spins consequently has a net magnetisation M and in the high temperature limit it can be expressed as

$$M_0 = \chi_0 B_0 \tag{1.1}$$

where χ_0 is the static nuclear susceptibility and is proportional to $1/T$ (the Curie law) (Abragam, 1961).

A sample containing such a population of spins, when immersed in a static magnetic field (chosen to be the z direction), will have the spins precessing about the magnetic field at their Larmor frequency. If a magnetic field B_1 rotating at the Larmor frequency is applied in the $x-y$ plane perpendicular to the static field, the individual nuclear magnetic moments may be rotated with the result that the entire macroscopic magnetisation may be turned away from the static field. Once the perturbing field is removed, the spins will then relax back to their equilibrium orientations at a rate that can be detected.

The application of the rotating magnetic field is the basis of modern pulse NMR techniques. The rotating field, usually at radio frequencies of the order of 1000 times lower than

the static field, is applied for enough time to rotate the magnetisation through 90° (called a $\pi/2$ pulse) or 180° (or π pulse). Immediately after a 90° pulse, the magnetisation lies along the rotating y axis and will decay back to equilibrium due to two mechanisms. It will realign in the z direction as thermal equilibrium is regained and will dephase in the $x-y$ plane due to the field inhomogeneity. The decay of the magnetisation in the z direction is exponential, with the time taken for the magnetisation to realign being given by the time constant T_1, called the spin-lattice (or longitudinal) relaxation time. The decay in the $x-y$ plane may also be exponential with a time constant T_2, the spin-spin (or transverse) relaxation time. The decay rate for the magnetisation in the $x-y$ plane is usually larger than or equal to the decay rate for the recovery of the magnetisation along the z direction (Fukushima and Roeder, 1981) .

If the magnetisation is observed in the rotating frame of reference, i.e. in the rotating $x-y$ plane, then the magnetisation in the z direction will appear to be stationary. The equations describing the transformation from the laboratory frame to a frame rotating at the Larmor frequency cause the static field to disappear from the equations of motion of the magnetisation. A 90° pulse is applied to the system and as soon as the pulse is removed a steady field B_1 is applied out of phase with the pulse. The spins then precess about this field, and B_1 becomes analogous to the E_0 field in the laboratory frame. The relaxation rate in the rotating frame has the time constant $T_{1\rho}$.

In a bulk material the spins are able to diffuse due to thermal activity. The motion of these precessing spins will result in fluctuating magnetic dipolar interactions. It is these interactions that allow the z component of the non-equilibrium magnetisation to recover to its equilibrium value. For a spin to align itself with the applied field energy must be transferred, so the rate at which the magnetisation recovery occurs depends on the mechanisms available for the spins to transfer energy to something else, namely the lattice. The mechanisms include rotations, vibrations and translations of the spins, so that the examination of the relaxation rates can give valuable information about the motion of the spins. The relaxation rate in the rotating frame will be most strongly affected by motions occurring at the Larmor frequency in the rotating frame, thus making analysis in this frame sensitive to slow motions in the kHz frequency region rather than the MHz region of the laboratory frame.

The purpose of this thesis is to examine the nuclear spin relaxation rates for diffusion in a disordered system. This is complicated as the presence of the disorder means that the

spins no longer diffuse about the system in a simple, regular manner. The way in which the disorder is manifest in the system is difficult to know exactly and the modelling can be difficult and time consuming for a large system with many spins present. For this thesis it was decided to examine the relaxation rates by modelling the diffusion exactly for a small, finite system at a low concentration of spins. The time constants T_1 and $T_{1\rho}$ can then be calculated exactly and compared to both experimental and theoretical work carried out on much larger systems. The purpose of this was to see how accurately a small system could model the real, large scale systems and to gain some insight into the mechanisms behind the diffusion process in a disordered system.

The simplest model for diffusion is to consider a single spin on an otherwise empty lattice that is diffusing by making jumps to nearest-neighbour sites. The jumps are assumed to be discrete and occurring instantaneously from one site to another. Site blocking by other spins, an important consideration for any real system, is also considered when calculating the probabilities of spins jumping to vacant sites on the system. This is called the simple hopping model.

The next section describes a particular example to which the theory can be applied: that of hydrogen in metals.

1.2 Hydrogen in Metals

Hydrogen in metals is an example of diffusion through both crystalline and non-crystalline systems. The reasons behind the study of hydrogen in metals are twofold. Firstly, there is the purely scientific pursuit of knowledge: secondly, there are the practical applications of such systems.

Practical applications are derived from the fact that the thermodynamic properties of the absorption process of hydrogen into metallic lattices can be put into use in energy storage devices and heat pumps. Hydrogen is usually absorbed under conditions of reasonable temperature and pressure, and similar processes can be used to extract the hydrogen when required. It has been found that under standard temperature and pressure, the hydrogen will remain trapped in the metallic lattice for long periods of time (McDowell, 1993). Commercial applications have so far been largely limited due to engineering difficulties, with an exception being the development of the nickel-hydrogen battery, a replacement for the NiCad battery.

When hydrogen is absorbed into a metallic lattice, it does so as an interstitial defect. The number of interstitial sites available depends on the structure of the lattice; for example in the FCC structure the interstitial locations between atoms are the centres of tetrahedra ("T" sites, giving eight possible sites per unit cell) or the centres of octahedra ("O" sites, with four sites per unit cell). As a result of the large number of possible sites for the hydrogen to occupy, a very large quantity of hydrogen can be absorbed into a lattice, up to a point where, in some cases, the density can exceed that of liquid hydrogen.

Although there are a large number of interstitial sites, not all will necessarily be filled by hydrogen. Palladium, for example, can only absorb up to a relative concentration of hydrogen atoms of 0.6, i.e. giving a stoichiometry of $PdH_{0.6}$, rather than a ratio of 1.0 or greater if all the interstitial sites were filled. The amount of hydrogen that can be absorbed is limited by a number of factors, including the electrostatic repulsion of the hydrogen atoms as they approach each other, and by the effect the absorption of hydrogen has on the electronic structure of the host. In general, two hydrogen atoms cannot be found in sites that are closer than 2.1 Å, a condition known as the Switendick criterion (Switendick, 1979).

The structure of the lattice affects the way in which the hydrogen diffuses. If the host is not a perfect lattice, that is, it contains some degree of disorder, then the diffusion will be greatly affected. The next section details the kinds of disorder seen in metal alloys.

1.3 Types of Disorder

A disordered system is one that does not contain any long range order. There are several ways in which disorder may be classified, the main ones being structural disorder, site energy disorder and saddle point energy disorder. In general all three will be present in a sample.

Structural disorder occurs when the atoms of the system are displaced from their ordered FCC, BCC, etc structure. Structural defects are classified by their dimensionality as point defects (those of atomic size or effectively zero dimension), linear defects or dislocations (dimension one), surfaces and interfaces (dimension two) and voids, precipitates, inclusions, etc (dimension three) (Allnatt and Lidiard, 1993).

Point defects are principally vacant lattice sites, interstitial atoms, foreign atoms and, in compounds, what are called wrong atoms. These are where atoms are present in one sub-lattice that properly belong on another.

Dislocations are a result of the way a specimen has been prepared and handled. They may contain straight sections, but are generally curved. The distortion of the crystal structure around a dislocation boundary can become an internal source of vacancies and interstitials. In practice most solids will contain a fairly high density of dislocations – around 10^9 to 10^{12} lines cutting each square metre of area.

External surfaces interrupt the lattice periodicity of the otherwise perfect infinite crystal and can act as sources or sinks of point defects. An important interface defect is the stacking fault, where the correct relationship between successive lattice planes is upset.

Three-dimensional imperfections include voids, colloids (small metallic particles in a compound host), bubbles, other precipitate phases and inclusions. These are most significant in diffusion as they can act as sources and sinks of point defects.

Of these four classes of imperfections only point defects may exist in a state of thermodynamic equilibrium. In general, point defect concentrations increase rapidly with temperature, decrease with pressure and in compounds, increase with departures from stoichiometry.

Site energy disorder occurs when the potential energy of the atoms in the system varies from site to site. This creates potential wells, where a diffusing atom can become trapped, as well as sites that allow the rapid hopping of atoms due to their relatively shallow potential well.

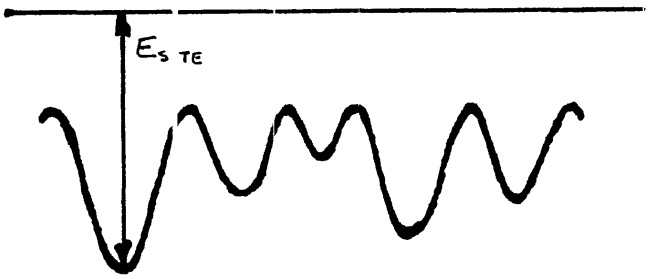

Figure 1.1: Site Energy Disorder

Saddle point energy disorder is where the potential barrier that must be overcome for a atom to jump from site to site varies from direction to direction. This can result in a site having a jump from it blocked by a large potential barrier in one direction, but having another direction with a small barrier, thus allowing diffusion to continue.

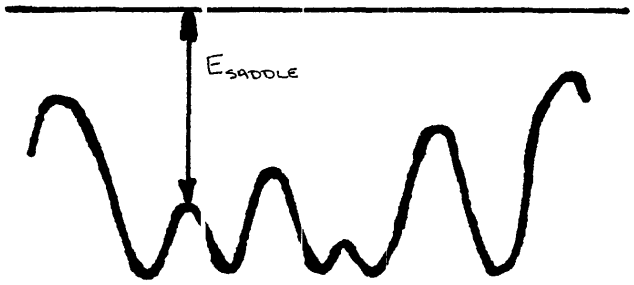

Figure 1.2 Saddle Point Energy Disorder

In a sample all of these classifications of defects will be present. To simplify the modelling of diffusion through disordered systems it is often assumed that there is only one defect mechanism present. Structural disorder is most often ignored and models of energy disorder often use only site energy disorder or saddle point energy disorder. The system used in this thesis models small systems with either site energy or saddle point energy disorder, and no structural disorder. While this is quite a simplification of the real situation it allows some determination of which kinds of disorder have the greatest influence on the diffusion through disordered systems.

The next chapter will detail the derivation of the relaxation rates as well as examining the work that has been done in the past on ordered and disordered systems. Chapter 3 will give the basic theory of applying the model of finite systems to both ordered and disordered systems, and will detail the testing of the model on an ordered, infinite system. Chapter 4 will build on these results, applying them to a disordered system, and Chapter 5 will conclude the thesis.

Chapter 2

Review

2.1 Nuclear Spin Relaxation Rates

Relaxation by dipolar coupling can be analysed by treating the dipole dipole interaction as a perturbation of the nuclear Zeeman Hamiltonian (Abragam, 1961). The dipole-dipole interaction between two spins I and S can be written

$$\hbar\mathcal{H}_1 = \sum_{q=-2}^{2} F^{(q)} A^{(q)} \tag{2.1}$$

where the $F^{(q)}$ are random functions of the relative positions of two spins, defined as

$$F^{(q)} = \frac{d_q Y_{2q}(\Omega)}{r^3}. \tag{2.2}$$

The vector $\mathbf{r}$ is the separation of the two spins I and S, defined in spherical coordinates as $\mathbf{r} = (r, \Omega)$. The randomness of the functions $F^{(q)}$ arises from the diffusion that affects $\mathbf{r}$. $Y_{2q}(\Omega)$ are the normalised spherical harmonics defined relative to the direction of the applied magnetic field and d_q are constants such that $d_0^2 = 16\pi/5$, $d_1^2 = 8\pi/15$ and $d_2^2 = 32\pi/15$.

The $A^{(q)}$ are spin operators:

$$\begin{aligned} A^{(0)} &= \frac{1}{\sqrt{6}}\left\{-\frac{2}{3} I_z S_z + \frac{1}{6}\left(I_+ S_- + I_- S_+\right)\right\} \\ A^{(1)} &= \frac{1}{2}\left\{I_z S_+ + I_+ S_z\right\} \\ A^{(2)} &= \frac{1}{2} I_+ S_+ \end{aligned}$$

$$a = -\frac{3}{2}\gamma_I\gamma_S\hbar \tag{2.3}$$

where γ_I and γ_S are the nuclear gyromagnetic ratios for spins I and S respectively. The relations $F^{(q)} = F^{(-q)*}$ and $A^{(q)} = A^{(-q)\dagger}$ also hold.

The ensemble averaged correlation function, for both like- and unlike-spin magnetic dipolar interactions, is given by

$$G^{(q)}(t) = \sum_j \overline{F_{ij}^{(q)}(0)F_{ij}^{(q)*}(t)} \tag{2.4}$$

where the subscripts i and j represent the spins I and S respectively. The corresponding spectral density function is

$$\begin{aligned} J^{(q)}(\omega) &= \int_{-\infty}^{\infty} G^{(q)}(t)\exp(-i\omega t)dt \\ &= 2\int_0^{\infty} G^{(q)}(t)\cos(\omega t)dt. \end{aligned} \tag{2.5}$$

Writing S_z as I'_z to highlight the fact that the spins are like spins it can be shown that the macroscopic equation for spin-lattice relaxation of like spins has the form

$$\frac{d}{dt}\langle I_z + I'_z\rangle = -\frac{1}{T_1}\left\{\langle I_z + I'_z\rangle - \langle I_z + I'_z\rangle_0\right\} \tag{2.6}$$

with

$$\frac{1}{T_1} = R_1 = \frac{3}{2}\gamma^4\hbar^2 I(I+1)\left\{J^{(1)}(\omega_0) + J^{(2)}(2\omega_0)\right\}. \tag{2.7}$$

The examination of the amplitude of precessing magnetisation in a plane perpendicular to the applied magnetic field can be performed with similar methods. It leads to T_2 in terms of the spectral density functions $J^{(q)}(\omega)$, which can be written as

$$\frac{1}{T_2} = R_2 = \frac{3}{8}\gamma^4\hbar^2 I(I+1)\left\{J^{(2)}(2\omega_0) + 10J^{(1)}(\omega_0) + J^{(0)}(0)\right\} \tag{2.8}$$

and the relaxation rate in the rotating frame is given by

$$\frac{1}{T_{1\rho}} = R_{1\rho} = \frac{3}{8}\gamma^4\hbar^2 I(I+1)\left\{J^{(2)}(2\omega_0) + 10J^{(1)}(\omega_0) + J^{(0)}(2\omega_1)\right\} \tag{2.9}$$

where ω_0 is γB_0, the Larmor frequency in the stationary laboratory frame, while the frequency ω_1 is γB_1, the Larmor frequency in the rotating frame. It is generally of magnitude

1000 times less than that of the frequency ω_0. R_1, R_2 and $R_{1\rho}$ are called the relaxation rates.

The parameter q can take the values 0, ± 1 and ± 2, and corresponds physically to the possible transitions between nuclear Zeeman states of a pair of spins. The term $q = 0$ corresponds to classical local magnetic field effects and coupled transitions between the Zeeman states such that $\Delta m = +1$ for one spin and $\Delta m = -1$ for the second. These transitions will conserve the energy of the spin system for like spins, but not for unlike spins, so $q = 0$ will not occur in longitudinal relaxation for like spin systems. The terms $q = \pm 1$ correspond to $\Delta m = \pm 1$ for one spin and $\Delta m = 0$ for the second, while $q = \pm 2$ has for both spins either $\Delta m = +1$ or $\Delta m = -1$. These transitions change the component of magnetisation parallel to the direction of the magnetic field, so terms such as $J^{(1)}(\omega)$ and $J^{(2)}(\omega)$ will appear in relaxation rate expressions for both like and unlike spin dipolar interactions.

Using the above definitions the correlation functions may be expressed as (Sholl, 1993)

$$G^{(q)}(t) = \frac{d_q^2}{4\pi} \sum_{\alpha\beta} \frac{Y_{2q}(\Omega_\alpha) Y_{2q}^*(\Omega_\beta)}{r_\alpha^3 r_\beta^3} P_{eq}(\boldsymbol{r}_\alpha) \pi(\boldsymbol{r}_\alpha, \boldsymbol{r}_\beta, t) \tag{2.10}$$

and so the spectral density functions will be

$$J^{(q)}(\omega) = \frac{d_q^2}{4\pi} \sum_{\alpha\beta} \frac{Y_{2q}(\Omega_\alpha) Y_{2q}^*(\Omega_\beta)}{r_\alpha^3 r_\beta^3} P_{eq}(\boldsymbol{r}_\alpha) \tilde{\pi}(\boldsymbol{r}_\alpha, \boldsymbol{r}_\beta, \omega). \tag{2.11}$$

$\pi(\boldsymbol{r}_\alpha, \boldsymbol{r}_\beta, t)$ is the probability of the spins being separated by $\boldsymbol{r}_\beta$ at time t if they were initially separated by $\boldsymbol{r}_\alpha$. The term $\tilde{\pi}(\boldsymbol{r}_\alpha, \boldsymbol{r}_\beta, \omega)$ is the Fourier transform of the probability function $\pi(\boldsymbol{r}_\alpha, \boldsymbol{r}_\beta, t)$. $P_{eq}(\boldsymbol{r}_\alpha)$ is the equilibrium probability of finding a pair of spins separated by $\boldsymbol{r}_\alpha$. It is included to account for the fact that the jump rates out of a site due to site energy disorder, when present, are temperature dependent, so the initial distribution of spins on the lattice is not constant and can depend on temperature. In the absence of disorder $P_{eq}(\boldsymbol{r}_\alpha)$ is a constant equal to the average probability of occupation of a site.

The spherical harmonics in equations (2.10) and (2.11) are defined relative to the magnetic field direction as the z axis so that the correlation functions and thus the relaxation rates depend on the direction of the applied magnetic field relative to the crystal axis. For polycrystalline or amorphous systems, only the average over all field directions relative to the crystal axis can be observed. In this case it is sufficient to consider the spectral density functions averaged over all field directions, although strictly it is the magnetisation rather

than the spectral density functions that should be averaged but the difference between the two is usually small (Barton and Sholl, 1980).

The spherically averaged correlation functions are

$$G_{\alpha\nu}^{(q)}(t) = \frac{d_q^2}{4\pi} \sum_{\alpha\beta} \frac{P_2(\cos\theta_{\alpha\beta})}{r_\alpha^3 r_\beta^3} P_{eq}(\boldsymbol{r}_\alpha)\pi(\boldsymbol{r}_\alpha, \boldsymbol{r}_\beta, t) \tag{2.12}$$

and so the spherical averaged spectral density functions will be

$$\begin{aligned} J_{\alpha\nu}^{(q)}(\omega) &= \frac{d_q^2}{4\pi} \sum_{\alpha\beta} \frac{P_2(\cos\theta_{\alpha\beta})}{r_\alpha^3 r_\beta^3} P_{eq}(\boldsymbol{r}_\alpha)\tilde{\pi}(\boldsymbol{r}_\alpha, \boldsymbol{r}_\beta, \omega) \\ &= \frac{d_q^2}{4\pi} J(\omega). \end{aligned} \tag{2.13}$$

In these expressions $P_2(\cos\theta_{\alpha\beta})$ is the second Legendre polynomial, which results from the spherical harmonics averaged over all possible field directions, θ being the angle between $\boldsymbol{r}_\alpha$ and $\boldsymbol{r}_\beta$.

An important feature of the experimentally observed NMR data is the second moment of the lineshape, M_2. For a resonance curve described by a normalised shape function $f(\omega)$ with a maximum at a frequency ω_0, the nth moment M_n with respect to the point ω_0 is defined as (Abragam, 1961)

$$M_n = \int (\omega - \omega_0)^n f(\omega) d\omega. \tag{2.14}$$

If $f(\omega)$ is symmetrical with respect to ω_0 then all odd moments vanish. The knowledge of the moments gives some information on the shape of the resonance curve and in particular on the rate at which it falls down to zero in the wings, far away from ω_0.

The second moment of an NMR line is analogous to the moment of inertia of an object with the same shape as the line and contains line-broadening contributions only from pairwise interactions between spins (Fukushima and Roeder, 1981). In a homogeneously broadened system, each magnetic resonance line is symmetric and the normalised free induction decay (FID) can be expressed in a series

$$f(t) = 1 - M_2 t^2/2! + M_4 t^4/4! - M_6 t^6/6! + \ldots \tag{2.15}$$

where M_2, M_4, M_6, etc are the second, fourth, sixth, etc moments of the lineshape. From this it can be seen that the second moment describes the short time behaviour of the system.

In particular, the term $(1 - M_2 t^2/2!)$ describes the FID to within 1% when it has decayed to 89% of its initial height.

In solids the most commonly found lineshape is Gaussian, which yields a second moment given by $M_2 = \sigma^2$, where σ is the width of the Gaussian distribution. Where there is considerable motional narrowing the lineshape will be Lorentzian in form, which does not yield finite values for moments above the first moment M_1.

2.2 Spin Jump Rates

The spins in a lattice are able to diffuse due to the presence of defects, as outlined in the previous chapter, and due to thermal motion of the spins and host species. The mean time between jumps of a spin from one site to another is given by τ and is often of the activated, or Arrhenius form

$$\tau = \tau_0 \exp(E/kT) \tag{2.16}$$

where k is the Boltzmann constant T is the absolute temperature and τ_0 is a pre-exponential factor, which scales the jump time. E is an activation energy, related to the potential barrier that must be overcome for a spin to jump from one site to another. The spectral density functions will be dependent on this mean time τ between jumps, so it is convenient to write equations (2.12) and (2.13) as

$$\begin{aligned} G_{av}^{(q)}(t/\tau) &= \frac{d_q^2}{\pi} \sum_{\alpha\beta} \frac{P_2(\cos\theta_{\alpha\beta})}{r_\alpha^3 r_\beta^3} P_{eq}(\boldsymbol{r}_\alpha)\pi(\boldsymbol{r}_\alpha, \boldsymbol{r}_\beta, t/\tau) \\ J_{av}^{(q)}(\omega\tau) &= \frac{d_q^2}{\pi}\tau J(\omega\tau) \\ &= \frac{d_q^2}{\pi\omega}(\omega\tau) J(\omega\tau). \end{aligned} \tag{2.17}$$

The first form of the spectral density function gives the relaxation directly for a fixed τ, i.e. constant temperature, whereas the second form is useful for obtaining the relaxation rates as a function of temperature for a fixed frequency, as is usual in experiments.

For an ordered system each site is at the same potential, so that the diffusion throughout is characterised by a single jump time. In this case there is only one independent variable to consider for an experiment at a fixed frequency, the product $\omega\tau$, and equation (2.17) will give

the spectral density functions for a single spin diffusing about the lattice. If the correlation between two diffusing spins is being studied, then τ must be replaced by $\tau_d = \tau/2$.

When presenting the results of experimental or modelled NMR data the convention is to plot the relaxation rates R_i as $\ln(\omega R_i)$ versus $\ln(\omega\tau)$ so that the x-axis becomes proportional to $1/T$. The curves produced are, for an ordered system, symmetrical, with peaks at $\omega\tau = C$, where C is of the order of unity. Since there is only a single independent variable $\omega\tau$, a set of universal curves for the relaxation in the system under consideration can be drawn. A change in the frequency at which the experiment is performed will merely result in a scaling of the relaxation curves.

This is not the case for a disordered system. The curves are found to be no longer symmetric, the peak positions are shifted and changing the frequency will give a different set of results that are no longer merely a scaling effect. The presence of the disorder results in a spread of jump times across the system which leads to these effects. Previous work that has indicated such effects will be examined in Section 2.4, while Chapter 4 will show the results of the procedure adopted by this thesis when applied to a disordered system.

The theory of nuclear spin relaxation in ordered systems has been well studied and the next section will briefly review work in this area.

2.3 Ordered Systems

The simplest model for the spectral density functions in an ordered lattice is due to Bloembergen, Purcell and Pound (1948). It effectively assumes that the probability of a spin jumping from one state to another in a time t is given by

$$\pi(\boldsymbol{r}_\alpha, \boldsymbol{r}_\beta, t) = \delta_{\alpha\beta} \exp(-t/\tau_d) \tag{2.18}$$

where $\boldsymbol{r}_\alpha$ is the initial separation of a pair of spins, $\boldsymbol{r}_\beta$ is the final separation of the spins and τ_d is the mean time between jumps of one of the two spins. This is correct at time $t = 0$ but is an approximation for other times. The exponential $\exp(-t/\tau_d)$ is the probability of there being no jump in a time t. If τ_d is the mean time between jumps of a single spin the above equation is applicable for diffusion of unlike spins, for example, when one spin is fixed and another diffuses. For like spin diffusion, where both of a pair of spins diffuse, τ_d must be replaced by $\tau_d/2$. This BPP model corresponds physically to assuming that when a jump occurs the correlation between the two spins is destroyed. This would be the case if the

jump occurred over very large distances. In practice the jump distances are small enough for the correlation to be significant for several jumps of the diffusing spins. The model also does not take into account structural differences in the samples when modelling the diffusion, only including structural effects in the lattice summation. The spectral density function that corresponds to this model is

$$J(\omega\tau_d) = \frac{2}{1 + (\omega\tau_d)^2} \tag{2.19}$$

Torrey (1953) realised the BPP model gave no great insight into the diffusion mechanism and introduced a method of examining some of the microscopic details of the diffusion process. He used a random walk theory to account for the diffusion amongst lattice sites. The random walk theory used a Poisson distribution of jumps of a spin and the calculations were simplified by assuming one spin was fixed at the origin and the other diffused at twice the standard jump rate. The correlation function was written as an ensemble average, and then an expression was derived for the jump probability that involved the structure factor $A(\boldsymbol{\rho})$ and the probability function $f(\mathbf{r}_0)$ that depended on the nature of the diffusion taking place. The function $f(\mathbf{r}_0)$ is the initial spin density which depends on the circumstances of the particular problem. For uniform spin density $f(\mathbf{r}_0)$ is a constant while for lattice diffusion $f(\mathbf{r}_0)$ may be expressed as a sum over delta functions centered at the lattice points. The structure factor $A(\boldsymbol{\rho})$ is defined by inverting the three-dimensional Fourier transform of the probability of a spin being found at $\mathbf{r}$ and integrating over all $\mathbf{r}$:

$$A(\boldsymbol{\rho}) = \int P_1(\mathbf{r}) \exp(i\boldsymbol{\rho} \cdot \boldsymbol{r}) d\mathbf{r}. \tag{2.20}$$

$P_1(\mathbf{r})d\mathbf{r}$ is the probability that after one jump of the spin the new spin position will be at $\mathbf{r}$ in $d\mathbf{r}$ relative to its previous position. For a random walk on a space lattice the integral form of the structure factor is replaced by a summation term over all the nearest neighbour sites:

$$A(\boldsymbol{\rho}) = \frac{1}{z} \sum_{j=1}^{z} \exp(i\boldsymbol{\rho} \cdot \boldsymbol{r}_j) \tag{2.21}$$

where z is the number of nearest neighbours.

Torrey was not able to solve the equations exactly. By assuming isotropic diffusion, where $A(\boldsymbol{\rho})$ depends only on the magnitude of $\boldsymbol{\rho}$ and $f(\mathbf{r}_0) = n$, or uniform spin density, he was able to evaluate expressions for the spectral density functions in the low and high

temperature regions. These expressions then depended on the form of the structure factor chosen. For lattice diffusion an explicit solution could only be obtained for the low temperature region, where $\omega\tau \gg 1$. To cover the whole temperature range the approximation of isotropic diffusion where each jump distance was always the same was used. He found that this approximation gave good agreement with the explicit solution in the low temperature limit from which he concluded that his model gave an adequate approximation to the lattice diffusion problem.

Sholl (1974) applied this theory of lattice diffusion rigorously and compared the results to those of Torrey for the FCC lattice. The low and high temperature limit could be evaluated exactly, and numerical summations were used to obtain data between these limits. Sholl found that the differences between the exact analysis and the work of Torrey were quite small, with the maximum difference being 2.5%. Torrey's method of approximating the twelve nearest neighbours of the FCC lattice by spherical symmetry was expected to be less accurate for BCC and SC lattices due to their lower number of nearest neighbours.

Sholl (1975) later extended his exact analysis to BCC and FCC lattices and found that the agreement with results from Torrey's work was worse than that for the FCC lattice, as expected.

Wolf (1974) developed a model to calculate T_1 for a monovacancy system. This was the simple-hopping model applied in the limit where there is a low concentration of vacancies so that they do not interact in an infinite crystal. In comparing Wolf's results to the BPP and random-walk approximation, where a single particle diffuses as if on an empty lattice, Fedders and Sankey (1978) first used a mean-field approximation that included a correction term to the random-walk approximation to account for the fact that two particles could not occupy the same site. The calculations were done using a reciprocal-space formalism. The mean-field model assumes that any site a single particle might hop to has a probability $\bar{c}$, the concentration of vacancies, of being vacant. Thus the concentration of particles c is given by $c = 1 - \bar{c}$. This approximation is exact when $c \to 0$ or $c \to 1$. This lowered the relaxation rate T_1 by 11% at low frequencies and raised T_1 by 18% at high frequencies for a simple cubic lattice, indicating that the random walk model was inaccurate in these limits.

Fedders and Sankey then applied a more accurate multiple-scattering approximation which can be described as including the multiple scattering of the specific particle with a single vacancy (or other particle) exactly while the rest of the vacancies or particles are taken into account in a mean-field approximation. They found the results from this model

agreed well with the computer simulations of De Bruin and Murch (1973) and believed their data to be exact to between 4% and 8% when $c = 1$, better than 4% if $c < 0.9$ and approached 2% accuracy as $c \to 0$.

Barton and Sholl (1980) expanded on the work done by Fedders and Sankey. By taking the double Fourier transform and summing over the first Brillouin zone, as was done by Fedders and Sankey, care had to be taken in evaluating the lattice summations so that they would converge. Barton and Sholl used the planewise summation method, a more efficient system than the Ewald method employed by Fedders and Sankey.

The Brillouin zone summations were calculated by realising that the FCC or BCC lattice sites were sublattices of a SC lattice of half the FCC or BCC lattice parameter. Nearest-neighbour jumps on a FCC lattice then corresponded to second-nearest-neighbour jumps on a SC lattice and nearest-neighbour jumps on a BCC lattice corresponded to third-nearest-neighbour jumps on the SC lattice. This gave the advantage that the reciprocal-space summations were then evaluated over the simpler SC Brillouin zone. The mean-field and random-walk approximations could then be easily calculated over the whole temperature range for all three lattice structures. Barton and Sholl found that the results obtained by this method were in good agreement with those of Fedders and Sankey.

Faux, Ross and Sholl (1986) applied the Monte Carlo method to a variety of crystal structures over a wide range of spin concentrations. Forms of the correlation function and spectral density function could be found analytically for small and large values of t and $y = \omega\tau/2$ respectively, and these were used to analyse the Monte Carlo simulation data accurately. The simulation itself only included the relative motion of pairs of spins which were within a distance d of each other at time zero and at time t, so a correction term for other spin separations had to be included. This was evaluated in a similar way to the analysis used by Abragam (1961) in his calculation of spin-lattice relaxation rates due to translational diffusion in liquids.

The Monte Carlo data gave the correlation function $G(t)$ which then had to be Fourier transformed to give the spectral density function. Rather than use a least-squares fit to a sum of exponentials, which gave inaccurate results for the asymptotic behaviour of $G(t)$, the expression for $G(t)$ was rewritten so that it displayed the proper behaviour for large and small values of t, and gave an expression, the Fourier transform of which could be taken accurately.

For a concentration of $c = 0.01$ the results from the Monte Carlo simulation agreed

to better than 1% for $y < 1.8$ when compared with the mean-field theory calculations performed previously (Fedders and Sankey, 1978, Barton and Sholl, 1980). For larger values of y statistical errors in the calculations produced fluctuations in the Fourier transform and hence also in the relaxation rate. Other concentrations were also modelled with the result that reasonably accurate data could be generated, when compared to the analytic forms for large and small values of y. It was found as the concentration was varied the magnitude of the relaxation maximum varied by only approximately 6% over the whole range of c, but that the position of the maximum showed a strong concentration dependence.

Sholl (1988) recognised that tables of numerical data were often unwieldy and inconvenient to use when calculating relaxation rates. He proposed an analytic form of the spectral density function that was calculated to fit the tabulated data. The analytic form comprised seven parameters which could be evaluated for different concentrations and crystal structures by considering extremes such as $\omega\tau \gg 1$ and $\omega\tau \to 0$ as well as peak positions of the curves. Once a set of parameters was determined, the entire spectral density and relaxation curves could be generated. This produced a much simpler table of parameters based on the crystal structure and the spin concentration. The results were compared to known data in the high and low frequency limits, as well as peak positions. The analytical approximation was found to be accurate to better than 2%.

Monte Carlo simulations have been performed by Bustard (1980), based on a modified system used by Barton and Sholl. The simulation used over 6000 spins on a $20 \times 20 \times 20$ simple cubic lattice. The technique calculated the correlation function $G(t)$ at discrete times, approximating this description by a linear sum of exponentials and then Fourier transforming this exponential sum. They found that for large vacancy concentrations the computer model was highly inefficient due to a lack of spin pairs with a suitable number of first, second, and higher nearest distances for the lattice size used. Their results compared favourably with previous work. In the monovacancy limit and for the low frequency regime the results differed from Wolf's by less than 6%.

This is by no means an exhaustive analysis of the previous work done on ordered systems, but is to indicate that this is a well covered and understood area. Accurate analytic forms for diffusion in ordered systems are known for a wide range of crystal structures and spin concentrations and spectral density functions can be easily calculated.

Diffusion in a disordered system is much less well understood and a great deal of work has been done in attempting to understand the mechanisms behind the diffusion processes.

The next section will outline some of the work that has been done in this area.

2.4 Disordered Systems

There are many theories on the storage of hydrogen in amorphous systems and on the mechanisms behind the diffusion. The complex nature of disordered systems has led to a large number of different ways to analyse experimental data and model the diffusion.

2.4.1 Structural Analysis

The detailed structure of disordered systems is often uncertain. There are, however, some cases where models have been developed. An example is the work of Harris, Curtain and Tenhover (1987) who made electrochemical studies of early and late transition metal amorphous alloys. Based on their work they constructed a model for the absorption of hydrogen in the amorphous system. They proposed that for hydrogen storage in alloys of stoichiometry $A_{1-x}B_x$, the glass was a chemically random alloy with a structure composed of packed, distorted tetrahedra. The types of metal atoms at the vertices are given by $A_{4-n}B_n$, where $n = 1, 2, 3$ or 4, so that the number of each type of tetrahedra is proportional to the probability of choosing n B and $4 - n$ A atoms from the overall alloy composition. Due to extended site blocking effects not all of the available hydrogen sites may be occupied simultaneously, and Harris *et al.* proposed that the number of available hydrogen sites per metal atom was 1.9, independent of type of site, alloy composition and hydrogen concentration. Hydrogen interstitial sites were located at the "centres" of these tetrahedral units. They assumed the energetics of the hydrogen in the metal were independent of the temperature and independent of the value of x in the composition. This distribution enabled Harris *et al.* to predict the total hydrogen concentration for $Ni_{1-x}Zr_x$ alloys with an accuracy between 0 and 15% when compared to experimental results.

McDowell (1993) followed the same reasoning as Harris *et al.* when considering the way in which hydrogen was stored in amorphous $Ni_{0.33}$ $Zr_{0.67}H_x$. As nickel is a much poorer hydrogen absorber than zirconium McDowell suggested that the interstitial hydrogen would prefer sites with four zirconium nearest neighbours over those with more nickel as nearest neighbours. The probability that any site chosen at random in the amorphous $Ni_{1-y}Zr_yH_x$ system had n nearest zirconium neighbours was then given by the binomial theorem

$$P(\mathrm{Ni}_{4-n}\mathrm{Zr}_n) = \frac{4!}{n!(4-n)!}(1-y)^{4-n}y^n. \qquad (2.22)$$

This disorder would then lead to site energies that varied from site to site in the system.

Kirchheim (1982) used a Gaussian distribution to model the density of states of hydrogen in an amorphous system and derived an expression for the hydrogen chemical potential as a function of the mean free enthalpy of solution in terms of an error function. He verified this by making e.m.f measurements of the chemical potential of hydrogen of different concentrations in the metallic glass $\mathrm{Pd}_{77.5}\mathrm{Si}_{16.5}\mathrm{Cu}_6$ and $\mathrm{Ni}_{64}\mathrm{Zr}_{36}$. He found the experimental data fitted the error function form of the hydrogen chemical potential very well. A rectangular function for the density of states was also tried, but this failed to fit the experimental data. Kirchheim concluded that the measurements of the chemical potential of hydrogen in amorphous systems were very sensitive to the kind of density function used.

2.4.2 Data Interpretation and Curve Fitting

A large amount of experimental work has been done on nuclear spin relaxation due to diffusion in disordered systems. In an effort to understand the processes behind the diffusion and to explain the features of the observed relaxation rates researchers have examined specific parameters of the diffusion and fitted curves to the experimental relaxation rates curves. For example, Bowman, Attalla, Maeland and Johnson (1983) studied NMR data for amorphous $\mathrm{Zr_2PdH}_x$ as well as crystalline hydrides. They calculated correlation times over a wide range of temperatures for both systems from the minimum value of experimental relaxation rates in the rotating frame using an expression for $T_{1\rho}$ that had been found previously (Bowman, Rosker and Johnson, 1982). The amorphous system did not obey an Arrhenius plot: instead it appeared to be made up of three distinct straight line segments. This was interpreted as indicating three separate jump processes, perhaps along different diffusion pathways. The slope of part of the amorphous correlation time curves was similar to that for the crystalline systems which suggested that there were some similar diffusion pathways. This reasoning was incorrect since if data were taken at a different frequency for the same sample then the analysis would indicate that there were two different hopping rates for the same temperature. Bowman *et al.* had used the theory for an ordered system to analyse their data, which led to the incorrect interpretation of the results.

Majer, Renz and Barnes (1991) used pulsed-field-gradient NMR to study the diffusion

of hydrogen in zirconium hydrides. The concentrations of ZrH_x studied were for $x \approx 1.5$ to $x \approx 2$. They found that the jump rate departed from an Arrhenius behaviour at higher concentrations, a result that they interpreted as being due to a diffusion mechanism more complex than a simple diffusion model. They proposed that as $x \to 2$ the hydrogen began to occupy higher energy interstitial sites other than the tetrahedral sites occupied at lower concentrations. Their theory allowed the calculation of the diffusion constant in terms of jumps between the tetrahedral sites and the other higher energy sites, labelled X sites. When these were taken into account the diffusion constants calculated by the theory and the experimental values agreed quite well. Although they found that the percentage of X sites occupied was very small (less than 1% at 1000 K for $x = 1.98$), they played an important role in the diffusion process. This effect could account for the non-Arrhenius behaviour seen by Bowman *et al.* as their amorphous Zr_2PdH_x system had a hydrogen concentration of $x = 2.88$.

Markert, Cotts and Cotts (1987) took NMR data from an amorphous Zr-Rh hydride and attempted two different curve fitting procedures. Their experiments involved measuring the second moment of the lineshape M_2 and using this value in their calculations. Their initial curve fitting involved a single activation energy curve, which corresponded to the crystalline single jump rate model. As expected, this did not fit the data, giving peaks in the relaxation rates that were too high and slopes in the low temperature region that were too steep. The second model tried had a normalised distribution of activation energies, independent of temperature. The distribution used was Gaussian for values of the activation energy E_a less than 0.47eV and Lorentzian for $E_a > 0.47$eV with a maximum energy cut-off set at 0.67eV. By varying the width and peak value of the distribution used, and by using a value of the Korringa constant of 170 s K, a quite reasonable fit to the data was possible. The peak heights were well matched. However the narrowness of the relaxation rate maxima in the rotating frame $T_{1\rho}$ was not well fitted, and Markert *et al.* could offer no explanation for this narrowness.

McDowell (1993) carried out a large number of NMR studies of amorphous nickel-zirconium hydride for a range of hydrogen concentrations. He found the NMR relaxation peak positions and widths displayed a non-monotonic behaviour as a function of hydrogen concentration, a phenomenon not previously observed. He found that his samples were of good quality across the range of hydrogen concentrations and so eliminated the possibility of contaminated samples causing the non-monotonic behaviour.

As is universally found in relaxation rates for disordered systems McDowell's experimental relaxation curves were asymmetric, with the low temperature slope shallower than the high temperature slope. The peak positions were shifted and lowered when compared to the crystalline theory. Similar results were found by Walstedt *et al* (1977) who studied NMR data for Na β-alumina compounds.

The peak widths showed non-monotonic dependence on concentration, as did the peak positions. In a later paper in collaboration with Cotts (1995), McDowell measured the diffusion constant D, and from it found an estimate of the correlation time τ_c. For each hydrogen concentration, when τ_c was plotted as a function of reciprocal temperature, the data fell along straight lines, within experimental uncertainty. This indicated there was no localised hopping of the hydrogen which could have caused the non-monotonic behaviour observed.

McDowell fitted a spectral density function as given by Beckmann called the Havriliak-Negami spectral density function to his experimental data. It had the parameters δ, the degree to which the atomic motions were correlated, and the combination $\delta\epsilon$ which represented the barrier height distribution. $\delta\epsilon = 1$ corresponded to a unique barrier height and $\delta\epsilon = 0$ was the "greatest allowed" distribution. These parameters were varied arbitrarily until the best fit to the experimental data was obtained. This fitted the experimental data much better than the crystalline theories, although the lower hydrogen concentrations could not be fitted as well.

Following a similar approach to Markert *et al.* (1987), McDowell used a Gaussian distribution of activation energies to produce theoretical relaxation curves. The peak positions were first fitted, then the width parameter σ and mean jump rate τ_c^0 varied to best fit the data. Again it was found that the lower hydrogen concentrations could not be fitted by this curve as well as the higher concentrations.

It was thought that this poor fitting at low concentrations was caused by an overestimation of the second moment of magnetisation M_2. The measured value at low temperatures would be too large if the site energies were distributed so that the low energy sites were clustered together. This would mean the spins would be evenly distributed at high temperatures but clustered together at low temperatures causing an overestimate in the measurement of M_2.

One of the problems with the modelling of the hydrogen diffusion in these ways is interpreting the parameters used in the curve fitting. It can be assumed that the fitting

parameters $\langle E_a \rangle$ and Gaussian width σ correspond to the average barrier energy and the spread of barrier heights respectively, yet such a simplistic analysis does not give much of an insight to the mechanics of the diffusion. McDowell found that the NMR data yielded results that were dependent on the hydrogen concentration, yet the fitting parameters he used did not show a similar dependence.

Such a fitting model does not describe whether or not the energy distributions are in the saddle points or in the sites, or a combination of both. While it is known that both exist simultaneously in real samples, curve fitting does not say which type of energy distribution has the greatest effect on the diffusion through an amorphous system. A random distribution of jump rates also does not take into account possible correlations between the jump rates of neighbouring sites. The curve fitting procedures are phenomenological in nature only, in that they can describe the relaxation rates but give no fundamental information about the diffusion processes. One approach to gaining more details about the diffusion process involved in a disordered system is by the use of Monte Carlo simulations, which will be discussed in the next section.

2.4.3 Monte Carlo Simulations

In order to model the actual diffusion through disordered systems Monte Carlo simulations have been performed extensively. These allow greater examination of the physics behind the motion of the diffusing spins, allowing insights into the mechanisms behind the diffusion.

Crouch, Havill and Titman (1985) carried out NMR experiments on amorphous $Ni_{35}Ti_{65}H_{1.5}$. By subtracting the hyperfine contribution of the conduction electrons from the data they found a single activation energy for the sample over the range of temperatures, from which they argued that it was not necessary to assume a distribution of activation energies or jump rates to give a satisfactory account of the experimental data.

Crouch *et al.* also ran Monte Carlo simulations using a spatially disordered system with site energy disorder included in a separate run. The first simulation assumed that the jump probability was dependent on the jump distance, but that the overall jump probability was the same from site to site. The second simulation assumed the jump probability varying from site to site, but no particular jump direction was preferred. The model used was a 1000 site spatially disordered simple cubic lattice on which the spins were placed randomly at a concentration of 0.1, with 1000 jumps allowed for each simulation.

They found that the simulation with site energy disorder caused broadening of the

relaxation curves due to the variation of spin mobility from site to site, although this broadening was much smaller than previously thought. They concluded that very accurate measurements of the relaxation rate may be necessary to observe a distribution of jump rates or activation energies.

Richards and Shinar (1987) carried out Monte Carlo simulations on a simple cubic lattice of 1000 sites. They simulated both site and saddle point energy disorder, calculating the autocorrelation function for a single particle as they assumed the correlation was reasonably well destroyed after a single jump. The diffusion was simulated by choosing a nearest neighbour to a spin at random and allocating it a random number r between 0 and 1. For saddle point energy disorder the saddle point was allocated a rate given by $W = p\exp(-r\Delta)$, where p was a constant, r a random number between 0 and 1 and $\Delta = \ln(100)$, representing the width of the distribution. If $r \leq W$ then the jump took place, otherwise a new nearest neighbour was chosen at random and the process was repeated. For site energy disorder the energies were allocated in a similar manner and the same diffusion process was carried out. The data were collected from an average over 40000 different trials and Fourier transformed by fitting by a sum of exponentials.

They found that the saddle point energy disorder results differed little from BPP results while the site energy disorder displayed significant departure on the low temperature side of the T_1 minimum. They concluded that a distribution of site energies was far more effective in broadening and distorting the shape of the relaxation curves from NMR data.

Both the work of Crouch *et al.* and Richards *et al.* gave results that seemed to indicate that site energy disorder would cause greater broadening of the relaxation rates than saddle point energy disorder. This contradicts later work carried out with other Monte Carlo simulations. Both groups used random placement of the spins on the lattice before tracking the diffusion and calculating the correlation functions, rather than allowing the system to reach thermal equilibrium before making the calculations. This could account for the broadened behaviour observed for site energy disorder.

Adnani, Havill and Titman (1994) used a Monte Carlo simulation of 1000 traps situated on a simple cubic lattice seeded with spins at two concentrations of 0.1 and 0.9. Structural disorder was introduced by allowing the sites to move randomly with the maximum shift being 1/3 of a lattice spacing. This spatial disorder was kept constant for the entire simulation. The distribution of trap energies was chosen from a constant distribution between two limits so that the ratio between the greatest jump rate to the least was, for four separate

simulations, unity (no distribution), 10, 25 and 100. Data were collected after the system had been allowed to reach thermal equilibrium. The correlation data were fitted by trial and error by a sum of exponentials via minimising a sum of the squares of the deviations.

They found that the presence of a jump-rate distribution was only clearly discernible in concentrated samples, and that the pattern of jumps was different in dilute and concentrated systems. In the dilute system the spins mainly occupied the deeper traps and on diffusing encountered several shallower traps before meeting another deep one. This meant the spins took several hops to be decorrelated, whereas in the concentrated system the spins became decorrelated after a single jump.

Adnani *et al.* examined a model where the energy disorder was independent of temperature but the jump rates were dependent on temperature. By developing a locus of curves they were able to generate relaxation curves that were mostly symmetrical about the relaxation peak, a feature that was not expected from theoretical studies which said that the temperature dependence on the low temperature sides of the peak is generally smaller.

Adnani (1994) performed quasielastic neutron scattering and NMR experiments on amorphous $Zr_4PdH_{0.8}$ and $Zr_3PdH_{0.6}$ and attempted to fit a theoretical model to the results. No details of the model were given, other than it was performed via Monte Carlo simulations on a spatially and energetically disordered lattice initially at thermal equilibrium.

The modelled curves did not fit the experimental data, which Adnani explained was due to the way the hydrogen was distributed in the alloy. In the model the hydrogen was distributed randomly, whereas the alloy was a zirconium rich one which would have hydrogen coordinated more strongly around the tetrahedral Zr sites. He applied Torrey's theory to the measured data and the results seemed to indicate two activation energies in the samples at different temperatures.

McDowell (1993) used a Gaussian distribution of both site and saddle point energy disorder in his Monte Carlo simulations. The rate for each possible hop event in the system was given by

$$\Gamma_j = \Gamma_0 \exp(-(E_{saddle_j} - E_{site})/kT) \tag{2.23}$$

where Γ_j was the rate for the j^{th} hop event, E_{site} was the initial site energy and E_{saddle_j} was the saddle point barrier energy for the j^{th} hop. Γ_0 was the rate prefactor that set the overall time scale of the simulation. The spins were placed on the lattice either by filling sites at random, which corresponded to infinite temperature, or by filling sites from the

lowest energy upwards, which gave the initial condition as $T = 0$. In either case the spins were allowed to make a number of jumps so that thermal equilibrium was achieved. To move the spins the total rate even for the next event to occur somewhere in the system was calculated using

$$\Gamma = \sum \Gamma_j \tag{2.24}$$

where jumps to blocked sites were not included in the summation.

To find the spectral density functions from the correlation data of the simulations the Fourier transform of a piece-wise constant function had to be evaluated. To calculate this accurately McDowell used an averaged-rate approach which applies a probability density function to the discrete time intervals in the correlation function. By choosing an accurate value of this function the spectral density function could be obtained quickly and accurately. McDowell found that the simulations with site energy disorder produced symmetric relaxation peaks, whereas the saddle point energy disorder gave asymmetric peaks, which was consistent with his experimental data. By running the analysis for different concentrations on a 500 site FCC lattice he found that as the disorder was increased, the peaks in the saddle point energy disorder system were shifted to lower temperatures and the asymmetry increased. For site energy disorder the peaks were shifted slightly to higher temperatures and no asymmetry was found. The explanation for this was that increasing the saddle point energy disorder provided lower and lower energy pathways for atomic motion, while increasing site energy disorder tended to trap the spins in their sites more and more strongly.

The dwell time for saddle point energy disorder showed a strong non-Arrhenius behaviour, which McDowell thought explained the asymmetry seen in the relaxation plots. The site energy disorder dwell times followed an Arrhenius distribution exactly.

There are several disadvantages with using the Monte Carlo simulation method. It requires a large amount of computing time to calculate the correlation functions for the diffusion process, and very slowly diffusing spins can cause errors in the calculations. The correlation data then must be Fourier transformed to give the spectral density functions and the methods employed to transform the data (for example, least squares fitting by a sum of three exponentials (Richards and Shinar, 1987)) may introduce further errors. As can be seen from the above summary of previous work, the conclusions drawn from the Monte Carlo simulations may be very different due to the different diffusion models.

The approach to be followed in this thesis is quite different to the curve fitting and

Monte Carlo work that has been described. The spectral density functions for diffusion on a disordered system will be found by modelling the diffusion exactly for a low concentration of spins on a small, finite system. The diffusion will be for two spins on a simple cubic lattice with either site or saddle point energy disorder. The advantage of this over Monte Carlo simulations is that the computing time will be very much reduced and the calculations of the spectral density functions will be exact. The theory, which will be described in the next chapter, will be such that no numerical Fourier transform methods will be needed to obtain the spectral density functions. It will also provide information on the mechanisms behind the diffusion process, something that the curve fitting procedures are not capable of doing.

Chapter 3

Spectral Density Functions in Finite Systems

3.1 Introduction

As outlined in §2.1 of the previous chapter, the correlation function $G^{(q)}(t/\tau)$ and the spectral density function $J^{(q)}(\omega\tau)$ may be written as (dropping the "av" subscript)

$$\begin{aligned} G^{(q)}(t/\tau) &= \frac{c_q^2}{4\pi}\sum_{\alpha\beta}\frac{P_2(\cos\theta_{\alpha\beta})}{r_\alpha^3 r_\beta^3}P_{eq}(\boldsymbol{r}_\alpha)\pi(\boldsymbol{r}_\alpha,\boldsymbol{r}_\beta,t/\tau) \\ J^{(q)}(\omega\tau) &= \frac{c_q^2}{4\pi}\sum_{\alpha\beta}\frac{P_2(\cos\theta_{\alpha\beta})}{r_\alpha^3 r_\beta^3}P_{eq}(\boldsymbol{r}_\alpha)\tilde{\pi}(\boldsymbol{r}_\alpha,\boldsymbol{r}_\beta,\omega\tau). \end{aligned} \tag{3.1}$$

The purpose of this thesis is to evaluate the spectral density functions for disordered systems by modelling the diffusion exactly on a small, finite system for a low concentration of spins. It will be shown that the small system analysis, when suitably scaled, is a good approximation to an infinite system, except in the high temperature limit, thus demonstrating the validity of the procedure. The results from this approach may then be compared to other systems to test the results obtained from them. The advantage of using a small system is that the computing time required to calculate the relaxation rates would be quite small, as compared to the large amount of time required for Monte Carlo simulations.

There are three important points to be noted. The first is that although structural disorder, in terms of the variations in jump distances for the spins, does exist in a real

system, it will be ignored in the model. Instead, a simple cubic lattice of varying size with site or saddle point energy disorder only will be used. This is a simplification of the real system, although there is some evidence that the presence of structural disorder has little effect on the relaxation rates (Havlin and Avraham, 1987).

The second is that although the purpose of this thesis is to examine disordered systems, the focus of this chapter will be on an examination of an ordered system, one that is characterised by a single jump time τ. This was done as the theory behind nuclear spin relaxation in an ordered SC lattice is known to a high accuracy and so could be used to provide a check on the validity of the small finite system model. The simple cubic lattice will also be used for the disordered system, with the disorder simulated by the inclusion of site and saddle point energy disorder only.

Thirdly, the thesis will model the diffusion in the low concentration limit only. By calculating the spectral density functions for two spins on the SC lattice the computations may be done rapidly and exactly. The results are therefore only valid in the low concentration limit. The results could, however, in principle be extended to general concentrations.

This chapter will detail the theory behind the small finite system model, and it's application to a small system. The results will then be compared to a known accurate analytic expression for the diffusion on an infinite ordered SC lattice. The final section will detail how a distribution of jump rates may be included in the theory for the small finite system model.

3.2 The Rate Equation for Populations

The term $\pi(\boldsymbol{r}_\alpha, \boldsymbol{r}_\beta, t/\tau)$ in equation (3.1) represents the way in which the spins are diffusing in the system and presents the main difficulty in modelling ordered and disordered systems. It can be modelled in terms of the jump rates of the spins in the following way.

Since the mean time of residence of spins on the sites of the lattice is long compared with the flight times between lattice sites, the jumps may be treated as occurring instantaneously. When considering like-spin or unlike-spin interactions, the spatial position of the spins i and j will be referred to as the state of the spins, indicated by the vector $\mathbf{r}_{ij}$ or $\boldsymbol{r}_\alpha$ where α is the state of the system. For like-spin interactions the orientation of the spins is not important, i.e. the state $\mathbf{r}_{ij}$ is the same as the state $\mathbf{r}_{ji}$. A jump of either of the spins will cause a transition from one state to another. The number of possible states N of a system

for like-spin diffusion on a finite simple cubic lattice with n sites is given by the number of ways of choosing 2 sites regardless of order from a set of n sites:

$$\begin{aligned} N(\text{states}) &= \frac{n!}{2!(n-2)!} \\ &= \frac{n(n-1)}{2}. \end{aligned} \tag{3.2}$$

The frequency of the transition from an initial state α to a final state β may be defined as $w_{\beta\alpha}$. It is assumed that the transition frequencies depend on the initial and final states only, and are independent of the previous history.

By defining the probability $p_\alpha(t)$ to be the time dependent probability that the system is in a state α, then the equation governing the evolution of $p_\alpha(t)$ can be written as (Allnatt and Lidiard, 1993)

$$\frac{dp_\alpha}{dt} = -\sum_{\beta\neq\alpha} w_{\beta\alpha}p_\alpha + \sum_{\beta\neq\alpha} w_{\alpha\beta}p_\beta. \tag{3.3}$$

This is called the master equation for populations. The first term on the right represents the rate at which systems are leaving state α for other states, while the second term gives the rate at which they are arriving in α from other states. This equation can be written in matrix form as

$$\frac{d\mathbf{p}}{dt} = -\mathbf{W}\mathbf{p} \tag{3.4}$$

where the matrix $\mathbf{p}$ is the matrix of occupation probabilities, and the square matrix $\mathbf{W}$ has elements

$$\begin{aligned} W_{\beta\alpha} &= -w_{\beta\alpha} \quad (\alpha \neq \beta) \\ W_{\alpha\alpha} &= \sum_{\beta\neq\alpha} w_{\beta\alpha}. \end{aligned} \tag{3.5}$$

Several important characteristics of these equations should be noted. From the definition of $\mathbf{W}$ it is clear that

$$\sum_\beta W_{\beta\alpha} = 0 \quad (\text{all } \alpha) \tag{3.6}$$

which is equivalent to the statement that probability is conserved. The matrix $\mathbf{W}$ will then always possess a left eigenvector $\tilde{\psi}$ such that

$$\tilde{\psi} = \begin{bmatrix} 1 & 1 & 1 & \dots & 1 \end{bmatrix} \tag{3.7}$$

where each element is unity and for which the corresponding eigenvalue is zero. It follows that the eigenvalues of $\mathbf{W}$ all have real parts greater than or equal to zero (Allnatt and Lidiard, 1993).

Furthermore, because any one row of $\mathbf{W}$ is equal to minus the sum of all the others then the determinant of $\mathbf{W}$ will be zero, i.e. $\mathbf{W}$ is a singular matrix. Care must then be taken in evaluating matrix equations containing $\mathbf{W}$ that have to be inverted.

The solution of equation (3.4) is of the form

$$\begin{aligned} \mathbf{p}(t) &= \exp(-\mathbf{W}t)\mathbf{p}(0) \\ &= \mathbf{G}(t)\mathbf{p}(0) \end{aligned} \tag{3.8}$$

where the matrix $\exp(-\mathbf{W}t)$ is defined by way of an exponential series. The matrix element $\exp(-\mathbf{W}t)_{\beta\alpha}$ gives the probability that the system will be in a state β at a time t if it was initially in state α at time zero. This solution corresponds to the probability function $\pi(\boldsymbol{r}_\alpha, \boldsymbol{r}_\beta, t)$, so a method for obtaining $\mathbf{G}(t)$ enables the spectral density functions, and hence the relaxation rates, to be calculated.

This theory is exact in the case of distinct eigenvalues. However, when there are degenerate eigenvalues, this approach of calculating the eigenvectors may no longer be valid. The general method for determining if the solutions to equation (3.18) are valid is to check whether or not the eigenvectors are linearly independent. The solution will be a linear combination of exponentials if a complete set of eigenvectors can be found for the degenerate eigenvalues, i.e., if for an eigenvalue with n level degeneracy there are n linearly independent eigenvectors, then the solution will be of the form $\sum_i c_i \exp(-\lambda_i t)$. The way to determine this is to calculate the determinant of the matrix of eigenvectors. If the determinant is non-zero, then the eigenvectors will be linearly independent, and the solution is a linear combination of exponentials. If the determinant is zero, then a polynomial solution must be sought by the use of the method of undetermined coefficients.

Consider, for example, the case where there is three-fold degeneracy in one of the eigenvalues in a system with n eigenvalues. It may be assumed that $\lambda_1 = \lambda_2 = \lambda_3 = \lambda$, and

all other eigenvalues are non-degenerate. In attempting to solve equation (3.4), assume a solution of the form

$$\mathbf{p} = (c_1\mathbf{p}_1 + c_2 t\mathbf{p}_2 + c_3 t^2\mathbf{p}_3)\exp(-\lambda t) + \sum_{n>3} c_n \exp(-\lambda_n t). \tag{3.9}$$

Substituting this into equation (3.4) and equating like powers of t yields the following sets of matrix equations:

$$\begin{aligned} \lambda\mathbf{p}_3 &= \mathbf{W}\mathbf{p}_3 \\ \lambda\mathbf{p}_2 + 2\mathbf{p}_3 &= \mathbf{W}\mathbf{p}_2 \\ \lambda\mathbf{p}_1 + \mathbf{p}_2 &= \mathbf{W}\mathbf{p}_1. \end{aligned} \tag{3.10}$$

These can then be solved sequentially to give the appropriate eigenvectors, and the constants can be found from the initial conditions.

There is a problem with attempting to solve this series of matrix equations. Because the matrix $\mathbf{W}$ is singular the solutions to equation (3.4) will not be linearly independent. This means that in attempting to solve equations (3.10) an inconsistent solution will be obtained. The problem may be overcome in the following way. By the conservation of probability

$$\sum_{\alpha} p_\alpha = 1 \tag{3.11}$$

so that the nth probability function p_n may be written as

$$p_n = 1 - \sum_{\alpha=1}^{n-1} p_\alpha. \tag{3.12}$$

Each of the differential equations in the matrix form of the master equation (3.4) may be written as

$$\frac{dp_\alpha}{dt} = -\sum_{\beta=1}^{n} W_{\alpha\beta}p_\beta \tag{3.13}$$

where α ranges from 1 to n. Substituting equation (3.12) into this yields

$$\frac{dp_\alpha}{dt} = -\sum_{\beta=1}^{n-1} W_{\alpha\beta}p_\beta - W_{\alpha n}\left(1 - \sum_{\alpha=1}^{n-1} p_\alpha\right)$$

$$= -\sum_{\beta=1}^{n-1} (W_{\alpha\beta} - W_{\alpha n})\, p_\beta - W_{\alpha n} \tag{3.14}$$

for $\alpha = 1$ to $n-1$. The steady state solution, or the equilibrium solution, $p_{\alpha eq}$ is found by setting the right hand side of this equation to zero and solving for p. Defining p'_α by

$$p_\alpha = p_{\alpha eq} + p'_\alpha \tag{3.15}$$

and substituting this back into equation (3.14) gives finally

$$\frac{dp'_\alpha}{dt} = -\sum_{\beta=1}^{n-1} (W_{\alpha\beta} - W_{\alpha n})\, p'_\beta \tag{3.16}$$

or in matrix form

$$\frac{d\mathbf{p}'(t)}{dt} = -\mathbf{W}' p'(0) \tag{3.17}$$

where the elements of $\mathbf{W}'$ are given by $W_{\alpha\beta} - W_{\alpha n}$. The matrix $\mathbf{W}'$ is no longer singular, resulting in a set of $n-1$ linearly independent solutions. By defining the square matrix $\mathbf{M}$ with columns which are the eigenvectors of the square matrix $\mathbf{W}'$, the equation (3.17) can be solved (Kelly, 1991) by

$$\begin{aligned}
\mathbf{p}'(t) &= \exp(-\mathbf{W}'t)\mathbf{p}'(0) \\
&= \exp(-\mathbf{M}\mathbf{M}^{-1}\mathbf{W}'\mathbf{M}\mathbf{M}^{-1}t)\mathbf{p}'(0) \\
&= \exp(-\mathbf{M}\mathbf{D}\mathbf{M}^{-1}t)\mathbf{p}'(0) \\
&= \mathbf{M}\exp(-\mathbf{D}t)\mathbf{M}^{-1}\mathbf{p}'(0) \\
&= \mathbf{G}'(t)\mathbf{p}'(0)
\end{aligned} \tag{3.18}$$

where the final step follows when the exponential is expressed as a Taylor series. The square matrix $\mathbf{D}$ is a diagonal matrix containing the eigenvalues of the matrix $\mathbf{W}'$. Finally, the solutions to equation (3.4) may be recovered by

$$\begin{aligned}
p_\alpha(t) &= p'_\alpha(t) + p_{\alpha eq} \qquad \alpha = 1 \text{ to } n-1 \\
p_n(t) &= 1 - \sum_{\alpha=1}^{n-1} p_\alpha .
\end{aligned} \tag{3.19}$$

This means that the solutions will be linear combinations of exponentials (or power series times exponentials) plus a constant term.

The matrix $\mathbf{W}'$ is a square matrix whose elements are calculated as shown in equation (3.5) from the probabilities of a pair of spins jumping from state α to state β in a single jump of one of the spins. For an ordered system each site is at the same potential so the jump probabilities are only modified by site blocking effects, and there is a single jump rate τ for the system. In a disordered system there will be site and saddle point energy disorder, so the jump probabilities will be affected by the disorder. The effect of this will be described in §3.5. Since $\mathbf{p}(0)$ is a column matrix containing the probabilities of particular states being occupied, then each column α of $\mathbf{G}(t)$ contains the probabilities of the system being in a particular final state at time t if it was initially in a state α.

Calculating $\mathbf{G}'(t)$ using equation (3.18) will yield a matrix whose terms are a linear combination of exponentials. Since the Fourier transform of the correlation function is required to find the spectral density functions, the diagonal exponential matrix will, once Fourier transformed, become a diagonal matrix of Lorentzians using

$$\begin{aligned} \mathcal{F}[\exp(-D_i t)] &= 2\int_0^\infty \cos(\omega t)\exp(-iD_i t)dt \\ &= \frac{2D_i}{D_i^2 + (\omega)^2}. \end{aligned} \tag{3.20}$$

If the Fourier transform of equation (3.19) is taken, then the constant term becomes a Dirac Delta function. This may be ignored in the calculations of the spectral density functions as the functions are required for values of the frequency other than $\omega = 0$.

Consider, for example, the case of two spins diffusing about a triangular, ordered lattice. The $\mathbf{W}$ matrix, assuming nearest neighbour jumps only, is

$$\mathbf{W} = \begin{pmatrix} 1 & -1/2 & -1/2 \\ -1/2 & 1 & -1/2 \\ -1/2 & -1/2 & 1 \end{pmatrix} \tag{3.21}$$

This matrix is singular, with the eigenvalues being 0, 3/2 and 3/2. By reducing this matrix $\mathbf{W}$ to $\mathbf{W}'$ the matrix will no longer be singular. The result is

$$\mathbf{W}' = \begin{pmatrix} 3/2 & 0 \\ 0 & 3/2 \end{pmatrix} \tag{3.22}$$

which has the eigenvalues of 3/2 and 3/2. By inspection, the solutions of this are

$$\begin{aligned} p_1'(t) &= p_1(0)\exp(-3t/2) \\ p_2'(t) &= p_2(0)\exp(-3t/2). \end{aligned} \tag{3.23}$$

With no disorder present the equilibrium solution will be $p_{eq} = 1/3$, so the full solutions to two spins diffusing on a three point ordered lattice are

$$\begin{aligned} p_1(t) &= p_1(0)\exp(-3t/2) + 1/3 \\ p_2(t) &= p_2(0)\exp(-3t/2) + 1/3 \\ p_3(t) &= 3 - (p_1(0) + p_2(0))\exp(-3t/2) \end{aligned} \tag{3.24}$$

Despite having degenerate eigenvalues the solutions contain no terms such as $t^n \exp(-\lambda t)$, other than $n = 0$. In the case of two spins on a triangular lattice, the eigenvectors for the reduced matrix $\mathbf{W}'$ are

$$\begin{bmatrix} 1 \\ 0 \end{bmatrix} \quad \begin{bmatrix} 0 \\ 1 \end{bmatrix} \tag{3.25}$$

with the determinant of the matrix made up from these eigenvectors being 1. As stated previously since the determinant of the eigenvalue matrix is non-zero then the eigenvectors are linearly independent and so equation (3.18) is a valid solution for two spins diffusing on a triangular lattice.

There are a few special cases to be considered. If the matrix $\mathbf{W}$ in equation (3.4) is Hermitian, then a complete set of eigenvectors can always be found, no matter the level of degeneracy of an eigenvalue. Since the matrices under consideration are always real, then the relevant condition would be that the matrix $\mathbf{W}$ must be real and symmetrical. If the matrix is not real and symmetrical, then it is still possible that a complete set of n eigenvectors can be found for an eigenvector with n level degeneracy. The test in this case is the calculation of the determinant of the eigenvector matrix.

By taking the determinant of the matrix made up from the eigenvectors of the matrix $\mathbf{W}$ it was possible to check the validity of the solutions of equation (3.18) for a matrix of any size. This was done for ordered diffusion on lattices up to a 36 site, simple cubic lattice, which in each case gave non-zero determinants of the eigenvector matrix. The

conclusion was that the method employed was valid for the systems under consideration as the determinants of the matrices were never zero.

3.3 Comparison to Known Systems

As a final test before comparing the model to a known analytic solution for a diffusion on an ordered, infinite system the model was compared to an expression for the high frequency, or low temperature limit (Barton and Sholl, 1980). For two spins on a triangular lattice the model was found to be accurate to 0.14% when $\omega\tau = 40$. With this the stage was set to compare the model to an infinite system. The next step was to evaluate the spectral density functions and relaxation rates over the whole temperature range and compare these to the results for the infinite system. It was important to test the model for a range of lattice sizes to see how quickly the model would approach the known infinite crystal results. If the approach was so slow as to require a very large lattice size then the computational method would be unacceptably slow in terms of computing time required to evaluate the matrix calculations. Since the size of the matrix $\mathbf{W}$ is proportional to n^2, where n is the number of lattice sites in the model, the matrices rapidly increase in size as more sites are added to the simulation. A reasonable approximation for a small number of sites to the infinite solution would validate the model for further study.

The exact solution chosen to compare with the model was the analytical expression derived by Sholl (1988). It has the form

$$\begin{aligned} J(\omega\tau) &= \frac{\tau}{a^6} g(y) \\ g(y) &= \frac{S}{a_1 + a_2 y^{\frac{1}{2}} + a_3 y^u + a_4 y^v + y^2} \\ y &= \omega\tau/2 \end{aligned} \tag{3.26}$$

where the values of S, a_1, a_2, a_3, a_4, u and v were determined by fitting by known analytic forms of $J(\omega\tau)$ for large and small values of y. The parameter a is the lattice parameter, which for a simple cubic structure is set to one. This model was known to be accurate for a wide range of hydrogen concentrations and lattice structures.

Two different sized systems were tried with the program. The first was a single cube structure, with eight sites, and the second a four cube structure, which had eighteen sites.

The spectral density functions were calculated in each case and compared to those of the exact expression.

It was found that although the form of the modelled spectral density functions was similar to that of the exact infinite solution, the magnitude of the modelled curves was significantly smaller. In fact, as the size of the lattice modelled was increased, the magnitude of the spectral density function decreased further. This is caused by the lattice summations over the finite system. A finite lattice structure will have edges, the atoms of which will not have, for the SC structure, six nearest neighbour atoms. As the lattice size is increased, the lattice sums will approach the infinite lattice sum of 8.4019.

In order to compare the results for the model with the infinite solution it was decided to normalise the sets of data. The normalisation factor used was $G(0)$, the value of the correlation function at time $t = 0$. For an infinite crystal the value of this is well known, being 8.4019. For the model the value was calculated for both systems by the summation

$$G(0) = \sum_{\alpha\beta} \frac{P_2(\cos\theta_{\alpha\beta})}{r_\alpha^3 r_\beta^3} P_{eq}(\boldsymbol{r}_\alpha) \tag{3.27}$$

which for one cube has a value of 0.18743, and for four cubes is 0.25550. After normalisation the data for the infinite crystal, one cube model and four cube model were plotted together. The original BPP distribution was also plotted as a comparison. The plots appear in figure 3.1. In each case the data are plotted as a function of $F(\omega\tau)$, defined as

$$F(\omega\tau) = \frac{J(\omega\tau)}{G(0)}. \tag{3.28}$$

As expected, the BPP approximation was a poor representation of the spectral density functions as compared to the Sholl approximation. This is because it assumes the relaxation is governed by a single exponential rather than a linear combination of exponentials. Physically, the BPP model says that the correlation between two spins is completely destroyed after a single jump of either of the spins.

The two solid curves, which represent the simulations for a one and four cube system, show good agreement with the results for the infinite system. Appreciable difference is found only for values of $\omega\tau$ less than one, which represents the region of long range diffusion. The model used here is not capable of modelling this region, which represents the high temperature side of the relaxation up to approximately the peak position. The model does give a good approximation to the low temperature side of the relaxation.

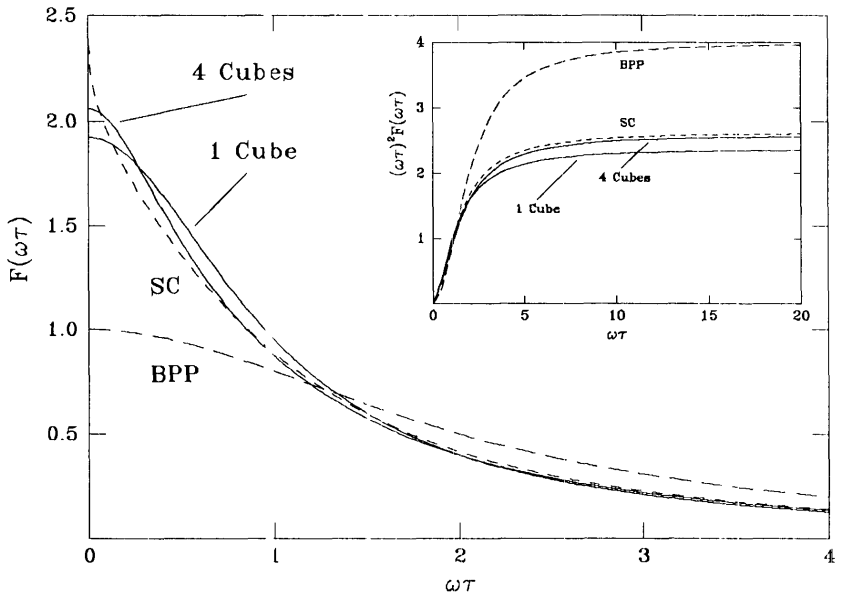

Figure 3.1: Comparison between normalised spectral density functions for known models and computational method.

The inset figure represents the approach of the models to the large $\omega\tau$ limit. It shows that the one and four cube simulation approach the analytic solution quite well for $\omega\tau \gg 1$, whereas the BPP model does not.

A point to note is that while the slope of the infinite approximation approaches infinity as $\omega\tau$ approaches zero, the computed values for the one and four cube system approach a finite value. The approach of the infinite case to infinity is due to long range diffusion which cannot be modelled by a small system. The value of $F'(0)$ for any finite sum will be zero because $F(\omega\tau)$ is a sum of Lorentzians and, as the size of the finite system is increased, the envelope of successive $F(\omega\tau)$ curves at small $\omega\tau$ will approach the function for the infinite system, reflecting the approach to long range diffusion.

On the basis of these results it can be said that a small finite system provides a reasonable approximation for $F(\omega\tau)$ for values of $\omega\tau \gtrsim 1$. This region corresponds physically to the high frequency or low temperature regime of NMR experiments, an area of considerable interest for disordered systems.

The time taken to calculate the curves is dependent on the size of the lattice used and the number or sub-intervals in the range of $\omega\tau$ used. The four cube system took a long time to model, so this system was the upper limit that could be practically used to generate a range of spectral density functions. The one cube system gave quite reasonable results with only a short calculation time of several minutes for the curve in figure 3.1, leading to the conclusion that this method of modelling a small finite system exactly yields a good approximation to the infinite case for $\omega\tau \gtrsim 1$.

3.4 Eigenvalue and Coefficient Analysis

The probability function $\pi(\boldsymbol{r}_\alpha, \boldsymbol{r}_\beta, t/\tau)$ that describes the time rate of change of the system from a state α to a state β in a time t/τ will be a matrix whose elements are linear combination of exponentials plus a constant. The correlation function $G(t/\tau)$ can then be expressed as a simple linear combination of exponentials and a constant

$$G(t/\tau) = \mathcal{C} + \sum_i a_i \exp(\lambda_i t/\tau) \tag{3.29}$$

where λ_i are the eigenvalues of the matrix $\mathbf{W}$ and a_i are the coefficients formed from the double summation in equation (3.). The eigenvalues and coefficients are characteristic of each lattice structure.

The Fourier transform of equation (3.29) will then be

$$J(\omega\tau) = \sum_i a_i \frac{2\lambda_i}{\lambda_i^2 + (\omega\tau)^2}. \tag{3.30}$$

As noted in §3.2 the ordered case will often give results that include degenerate eigenvalues but which still result in a solution for the spectral density function that is a linear combination of exponentials. For example, in the case of two spins diffusing about a single cube there are a total of 28 possible eigenvalues, the degeneracies being as shown in table 3.1.

As the size of the lattice is increased degeneracies are still evident in the ordered system, however, the level of degeneracy falls. For a 12 cube system, where there are 630 possible eigenvalues only one eigenvalue had a degeneracy of 4, while the others had degeneracies of 1 or 2, which resulted in 477 distinct eigenvalues. It was also of interest to note that not all of the coefficients a_i associated with a particular λ_i were of appreciable magnitude. A

Table 3.1: Eigenvalues and Degeneracy for Ordered Diffusion on One Cube

eigenvalue	degeneracy
0	1
2.1009	1
0.8991	1
0.4730	2
1.5270	2
0.3333	3
1.6666	3
1.3333	3
0.7940	3
1.5393	3
0.6666	6

significant number had values less than 10^{-6}, and so could be assumed to have little effect on the spectral densities if $\omega\tau \gg \lambda_i$, as is evident from equation (3.30). This could be shown by removing all eigenvalues with coefficients less than 10^{-6} and plotting equation (3.30) for this system as compared to the full set of eigenvalues and coefficients. For the 12 cube system it was found that there was virtually no difference between the two despite the number of terms in the summation being reduced from 477 to 206.

Once a set of eigenvalues and coefficients had been generated for a particular lattice structure they could then be used to generate the spectral density functions and relaxation rates under any conditions required for the ordered case. This was because the **W** matrix was unchanged by variations in temperature and changes in the value of ω or τ merely affected the scaling of the curves.

The shape of the distribution of eigenvalues and coefficients could be examined by plotting the data as histograms, such as in figure 3.2. The coefficient sum was found by adding together the values of the coefficients for each eigenvalue in the ranges specified by the x-axis.

This distribution was fairly typical for an ordered system. Generally there was a peak in the coefficients between eigenvalues of 0.5 and 0.9, with values of the coefficients falling off to either side. The eigenvalues range in size from 0 up to around 2.1, although not all had coefficients of magnitude 10^{-6} or greater.

A peak around $\lambda = 0.5$ was to be expected. If the simple BPP model is considered, it

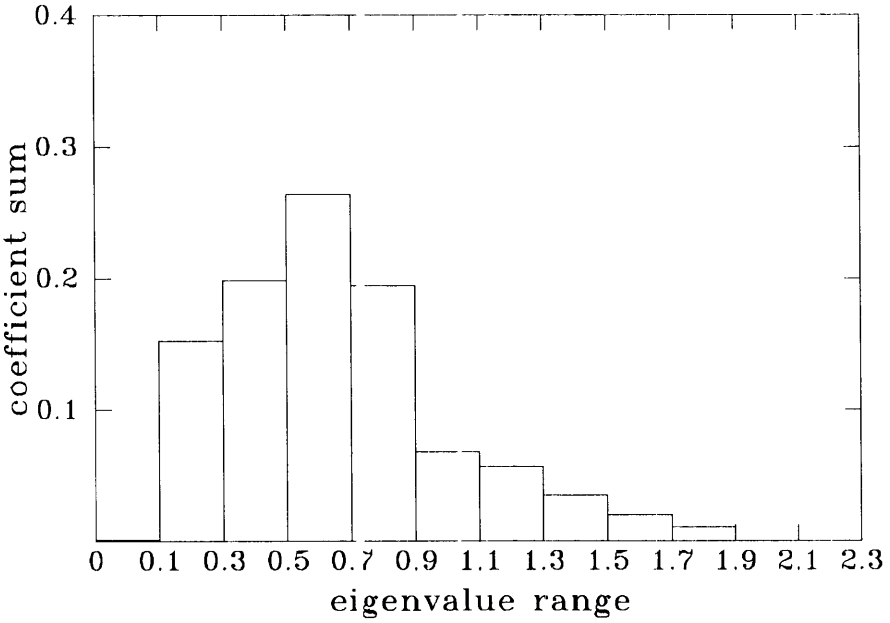

Figure 3.2: Histogram of eigenvalues and coefficients for a 12 cube, no disorder system.

assumes there will be a single jump rate and the correlation function is

$$G(t/\tau) = C\exp(-t/\tau). \tag{3.31}$$

The τ here is defined as $\frac{1}{2}\tau_d$, half the mean time between jumps of a single spin. This corresponds, if plotted as a histogram, to a delta function at $\lambda = 0.5$. The extra information contained in the histograms produced by the method outlined in this thesis demonstrates that while it shows similar behaviour to the BPP model, it is more accurate in evaluating the spectral density functions.

3.5 Modifications for a Disordered System

The calculation of the spectral density functions becomes more complicated when considering disordered systems as the disorder results in a spread of mean times between jumps across the sample. The jump time τ is no longer a single value, but will depend on the site and saddle point energy disorder (and to a lesser extent the structural disorder) present in

the sample.

The presence of the disorder will affect the rate equations. When there was no disorder the rate equations were only dependent on temperature implicitly. The mean time τ between jumps is given by $\tau = \tau_0 \exp(E/kT)$ which will be the same at all sites. When disorder is introduced the temperature dependence becomes explicit in the calculations of the jump probabilities $w_{\alpha\beta}$ from state β to state α. This does not overly complicate the calculations of the spectral density functions; they may be calculated at each temperature for a specific model of disorder. A plot of $\ln R$ versus $1/T$ then follows straightforwardly. For a sample with site and saddle point energy disorder only, the jump rate w_{ij}, defined as the reciprocal of the mean time between jumps τ_{ij}, from site i to site j will be given by

$$w_{ij} = \frac{1}{\tau_0} \exp(-(E_i - E_{ij})/kT) \tag{3.32}$$

where E_i is the energy of site i and E_{ij} is the energy of the saddle point between sites i and j.

The question, then, is how to present the data concisely in a general form. In an ordered system there is only the single independent parameter $\omega\tau$ which is only implicitly dependent on temperature. In a disordered system the explicit temperature dependence makes a choice of τ in this product more difficult. There are two possible choices. The first is to use the mean time between jumps of the disordered system $\overline{\tau}$, averaged over the whole spread of jump times in the system. The problem with using this mean jump time $\overline{\tau}$ is that it no longer obeys an Arrhenius relation, and so $\ln(\omega\overline{\tau})$ is no longer proportional to $1/T$. In order to produce theoretical plots equivalent to $\omega \ln R$ versus $1/T$ it is therefore necessary to separately calculate $\overline{\tau}$ as a function of temperature.

The other choice is to use the jump time τ_a which corresponds to the average energy of the distributions so that

$$\tau_a = \tau_0 \exp\left(\frac{E_b - E_s}{kT}\right) \tag{3.33}$$

where E_s and E_b are the average energies of the site and saddle point energies respectively. This assumes that τ_0 does not vary from site to site.

The disorder and spread of jump rates means that more than a single variable is needed to describe the general relaxation in a disordered system. By defining

$$\omega\tau_r = \omega\tau_0 \exp\left(\frac{E_b - E_s}{kT}\right) \tag{3.34}$$

then the combination of the two variables $\omega\tau_0$ and $(E_b - E_s)/kT$ can be used to describe the relaxation. For a specific value of $\omega\tau_0$ a set of universal relaxation curves can be generated, and when a new value of $\omega\tau_0$ is chosen a different set of universal curves can be drawn. This means that, in the disordered system, changing the frequency at which the experiment is performed will produce new information about the relaxation, unlike the ordered case where a change in the frequency merely changes the scaling of the curves. The same distribution function for the disorder was used as the parameters $\omega\tau_0$ and $(E_b - E_s)/kT$ were varied to produce the relaxation curves. Using a different distribution of site and saddle point energies would result in a different set of relaxation curves being generated.

The next chapter will extend the modelling to include site and saddle point energy disorder in the lattice, examining the effects this has on the form of the spectral density function and relaxation curves.

Chapter 4

Application to Disordered Systems

4.1 Introduction

The purpose of this Chapter is to apply the theory developed in Chapter 3 to some models of disordered systems. The first to be considered in §4.2 is a comparison with some experimental results for the metallic glass a-$Zr_3RhH_{3.5}$. This example was chosen because there is a good range of experimental data available and it has been thoroughly analysed using a modified BPP expression for the spectral density functions. The results using the analysis of small systems can therefore be obtained for a reasonably well characterised set of disorder parameters and compared with the results of the BPP analysis.

In §4.3 a method for expressing the spectral density function in terms of general dimensionless parameters will be developed. This allows a set of general curves to be drawn for the relaxation rates in a similar manner to ordered systems. The presence of disorder, however, introduces a second independent variable, so that a single set of universal curves will not describe all possible relaxation rates. This section will detail the introduction of this second independent variable and the way in which the data may be presented.

§4.4 will examine the distribution of eigenvalues and coefficients for a disordered system and the features of the relaxation curves that may be inferred from such distributions.

§4.5 will describe an attempt to combine a distribution of jump rates with a curve fitted to the eigenvalue and coefficient histograms for an ordered system as shown in Chapter 3. Such a model for disordered systems would have the advantages of being much quicker than detailed analysis and being derived from an exact analysis of an ordered system.

4.2 The Metallic Glass a-$Zr_3RhH_{3.5}$

An extensive set of proton spin-lattice relaxation rates, in both the laboratory and rotating frames, have been made by Markert, Cotts and Cotts (1987) on the metallic glass a-$Zr_3RhH_{3.5}$. The second moment of the lineshape M_2 was also measured at $T = 77$K and was found to be $M_2 = 7.8 \pm 0.8 \times 10^9 \text{sec}^{-2}$. The spin lattice relaxation times T_1 were measured at $(\omega_0/2\pi) = 38.9$MHz, 15.8MHz and 6.14MHz. The rotating frame times $T_{1\rho}$ were measured at $(\omega_0/2\pi) = 38.9$MHz with $(\omega_1/2\pi) = 45$kHz and 25kHz.

The relaxation rate curves from the experiments were asymmetric, with the slopes on the low temperature side of the maximum being shallower than on the high temperature side. At low temperatures and for an operating frequency of $(\omega_0/2\pi) = 38.9$ MHz, the decrease in T_1^{-1} was seen to be limited by the conduction electron mechanism $T_{1e}^{-1} = (T/K_r)$, where K_r is the Korringa constant, estimated to be about 170 ± 10 sK. This mechanism is independent of the NMR frequency.

Markert *et al.* calculated the maximum relaxation rates based on the work of Faux, Ross and Sholl (1986) which had considered only crystalline systems. They found that the experimental peak dipolar rates were less than the calculated rates for a given frequency and frame of reference. The difference between the two increased as the frequency (and therefore temperature) decreased. Markert *et al.* argued that this could be expected when there was a distribution of hydrogen hopping rates because the ratio $(\Delta E_a/k_bT)$, where ΔE_a is the width of the distribution function, increases as T decreases.

Markert *et al.* attempted two curve fitting procedures for their data. The first was for a single activation energy E_a independent of temperature, and the second was for a distribution of activation energies $G(E_a)$ independent of temperature. For the single E_a, or BPP model, both E_a and the jump rate τ_0 were varied until the best fit to the temperatures of the rate maxima were obtained. This resulted in curves that were too steep and where the maxima values were too great by a factor that increased as $(1000/T)$ increased.

The second model used a modified BPP expression to fit a distribution of activation energies to model the relaxation. The distribution was a normalised combination of a Gaussian and a Lorentzian with a maximum energy cut-off:

$$G_1(E_a) = \begin{cases} N \exp(-(E_a - E_p)^2/(2\sigma_1^2)) & E_a < E_p \\ N\left[1 + (E_a - E_p)^2/\sigma_2^2\right]^{-1} & E_p < E_a < E_c \\ 0 & E_a > E_c \end{cases} \quad (4.1)$$

where $E_p = 0.47$eV, $E_c = 0.67$eV, $\sigma_1 = 0.065$eV, $\sigma_2 = 0.04$ eV and N was a normalisation constant. The relaxation rates in the laboratory and rotating frame were calculated by evaluating the integral

$$T_n^{-1} = \int G(E_a) T_n^{-1}(E_a) dE_a. \quad (4.2)$$

where n represents either the laboratory frame rate T_1^{-1} or the rotating frame rate $T_{1\rho}^{-1}$. $T_n^{-1}(E_a)$ is the relaxation rate in either the laboratory or rotating frame at the energy E_a chosen from the distribution.

This distribution allowed Markert *et al.* to model their experimental data fairly well. There was good agreement between experimental and model maxima in the laboratory and rotating frames, although the experimental narrowness of the rotating frame peaks was not well fitted.

The equation (4.2) assumes a BPP function at each site and that the BPP function for each of these can be weighted by the probability distribution. These assumptions are not well justified. The weighting of the BPP functions by the probability distribution is arbitrary and gives no insight into the mechanisms behind the diffusion. The approach of the analysis of small finite systems has a much more rigorous basis. The choice of the meaning of the $G(E_a)$ function is important, as it can be used to model either site or saddle point energies, or both together. The small system model of this thesis will consider site and saddle point energies separately.

To compare the results of Markert *et al.* to the model used in this thesis, the energy distribution (4.1) was used to select a random set of energies for the simulations. For the first simulation the random energies were allocated to the sites of the lattice so that there was no deliberate correlation between the site energies. For the second simulation the random energies were allocated to the saddle points of the lattice, again with no deliberate attempt at correlating the spread of energies. Simulating the diffusion for site and saddle point energy disorder separately is an approximation to the real system but allows the examination of the effects of the two classes of disorder on the relaxation rates.

For site or saddle point energy disorder the barrier energies $E_{\alpha\beta}$ for diffusing from site α to site β were chosen from the distribution $G(E_a)$. The mean time between jumps was then defined as

$$\begin{aligned} \tau &= \tau_0 \exp(E_{\alpha\beta}/kT) \\ &= \tau_0 \exp(E_{av}/kT) \exp((E_{\alpha\beta} - E_{av})/kT) \end{aligned} \tag{4.3}$$

where E_{av} was set at 0.40eV. The overall jump times were then scaled by the product $\tau_0 \exp(E_{av}/kT)$ so that the jump times in these units are of order unity.

Several runs for each type of disorder were carried out so that a wide range of random distributions of energies were simulated. For each choice of jump rates, and at each temperature, the matrix **W** from equation (3.4) was calculated and the rate equations solved. This yielded the probability function $\tilde{\pi}(\boldsymbol{r}_\alpha, \boldsymbol{r}_\beta, \omega\tau)$. The equilibrium concentration $P_{eq}(\boldsymbol{r}_\alpha)$ was also calculated at each temperature. This had a different form for site and saddle point energy disorder. For saddle point energy disorder, each site was at the same energy level, so the normalised equilibrium distribution probability for saddle point energy disorder was the same regardless of temperature or disorder. For site energy disorder the equilibrium distribution was dependent on the temperature and the disorder present. The spectral density functions were calculated by summing over all initial and final states α and β respectively, with the second Legendre polynomial $P_2(\cos\theta_{\alpha\beta})$ calculated in each case. The results for both site and saddle point energy distributions, averaged over 40 simulations on an eight site lattice, are shown in figure 4. . The curves have been superimposed so they may be more easily compared.

The site energy disorder produces symmetric curves, whereas the saddle point energy distribution gives relaxation curves with appreciable asymmetry. Such asymmetry is often a characteristic of experimental relaxation curves, which would seem to indicate that saddle point energy disorder, at least for low concentration systems, is more significant than site energy disorder. Similar results were found by McDowell (1993) who used a Gaussian distribution of site and saddle point energy in Monte Carlo simulations. Interestingly, Richards and Shinar (1987) found the opposite was the case in their Monte Carlo simulations. They found that site energy disorder caused the relaxation curves to be broadened and that saddle point energy disorder had no such effect.

The a-$Zr_3RhH_{3.5}$ system is not a low hydrogen concentration system. As the hydrogen

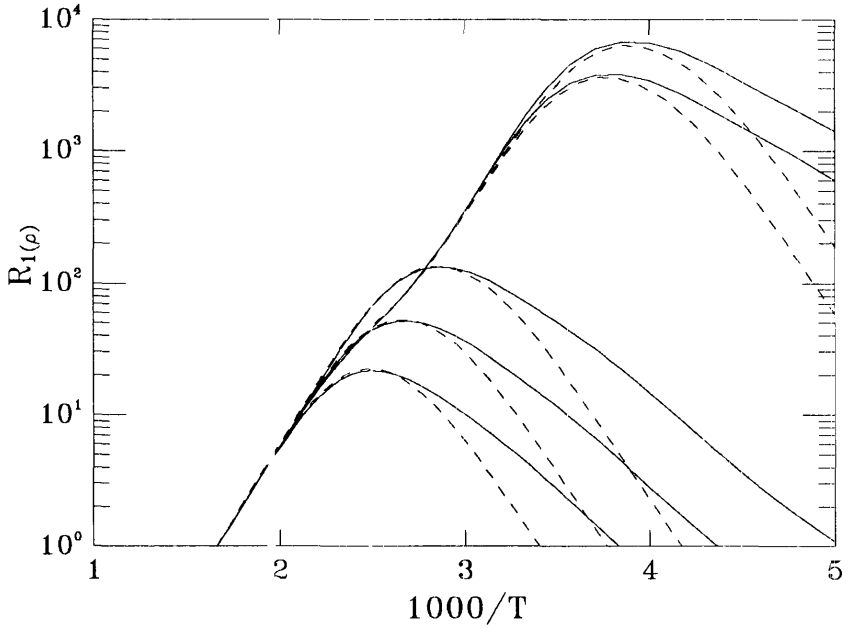

Figure 4.1: Calculated relaxation rates R_1 (lower group of curves) and $R_{1\rho}$ (upper group) for site energy disorder (dashed curves) and saddle point energy disorder (solid curves).

concentration increases the lower energy sites will be filled first, leaving the remaining hydrogen to diffuse over relatively shallow site energies. This could change the behaviour of the relaxation rates. A way to approximate high concentration effects using the present low concentration limit theory is to replace the calculated $P_{eq}(\boldsymbol{r}_\alpha)$ for site energy disorder by $P_{eq}(\boldsymbol{r}_\alpha) = 1/N$, where N is the number of sites in the system. The assumption of a constant equilibrium distribution of spins at any temperature corresponds physically to a high concentration of spins where the majority of deep potential sites are filled. The simulations for site energy disorder using this substitution produced curves that were asymmetric, similar to those produced by the saddle point energy disorder. These can be seen in figure 4.2.

This would indicate that a knowledge of the equilibrium distribution of spins is important in understanding the diffusion process. In the work done by Richards and Shinar, they seeded their Monte Carlo lattice randomly regardless of temperature and found that site energy disorder caused asymmetry in the relaxation curves rather than saddle point energy disorder. This random seeding corresponds to setting $P_{eq} = 1/N$. It is possible that if they had used a thermal equilibrium for the initial distribution of spins that they would have

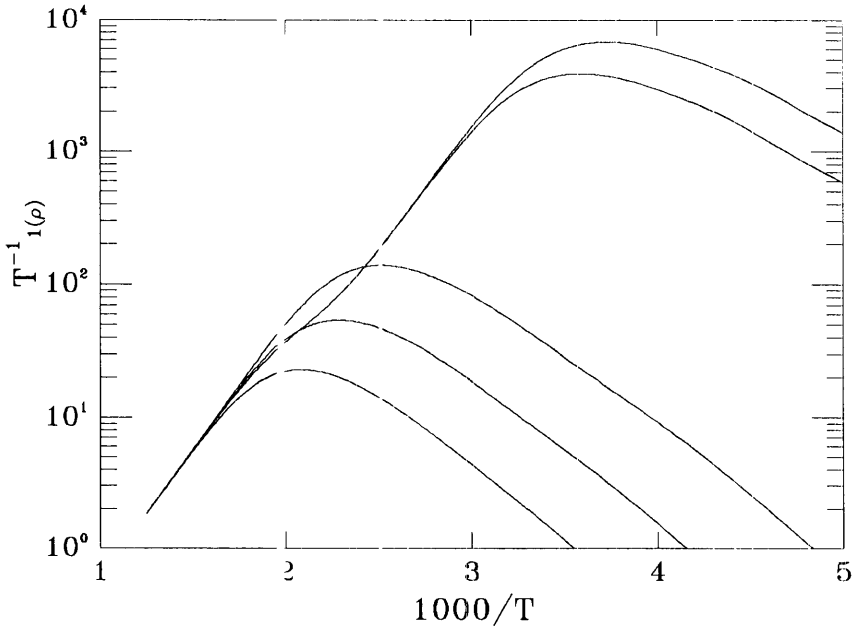

Figure 4.2: Calculated relaxation rates R_1 (lower group of curves) and $R_{1\rho}$ (upper group) for site energy disorder with $P_{eq}(\mathbf{r}_i) = 1/N$.

observed results similar to those in figure 4.1.

The difference in the sets of curves for site and saddle point energy disorder in the small finite system model may be explained in the following way. As the temperature decreases, the jump rate out of a particular site will also decrease. For site energy disorder, if a spin jumps into a deep potential well then it will see the same large energy barrier in any possible jump direction. At lower temperatures the spin will not have the energy to jump over the barrier and so will become trapped, slowing the relaxation rates. With saddle point energy disorder at lower temperatures a spin may see a large barrier energy in one direction, but there may be a much smaller barrier energy in another allowed jump direction. The spin can then jump over this smaller barrier and continue to diffuse through the system, thus enhancing the relaxation rate and leading to the asymmetric curves observed.

To compare the present results and those of Markert *et al.* calculated from their modified BPP model the two sets of data are plotted together in figure 4.3. The small system model, shown in the solid curves in the figure, is for saddle point energy disorder on a single cube system with the equilibrium term $P_{eq}(\boldsymbol{r}_\alpha)$ calculated as normal at each temperature. It can

be seen that the qualitative shapes of the curves are similar although there are differences in detail.

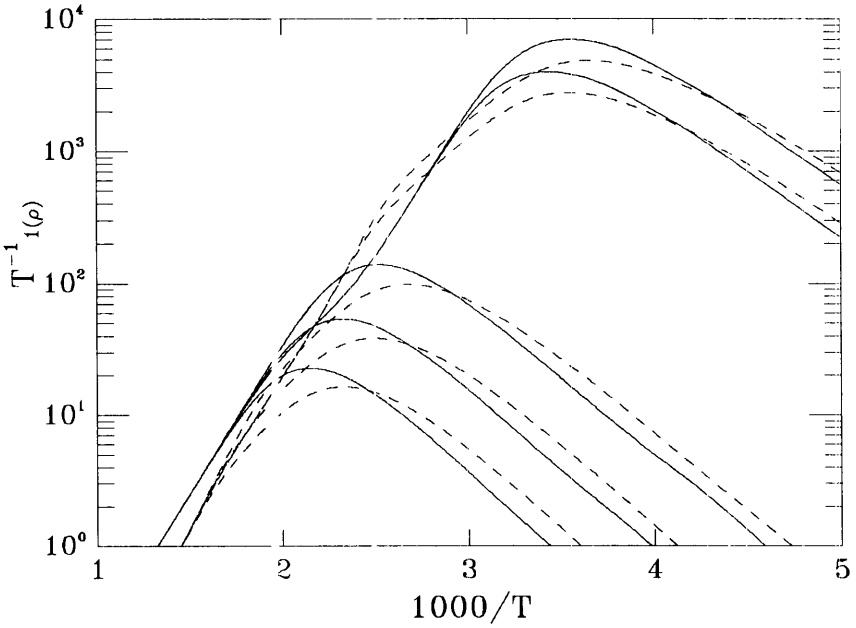

Figure 4.3: Comparison between MCC fitted curve (dashed lines) and small, finite system model (solid lines). The lower group of curves are for R_1, the upper for $R_{1\rho}$.

From this it can be concluded that the present approach can, in principle, explain experimentally observed asymmetric data. To fit the calculated curves to the experimental data would require adjustment of the parameters in the energy distribution $G(E_a)$ such as the Gaussian and Lorentzian widths σ_1 and σ_2 respectively, the peak energy position and the cut-off energy.

The results for the small system model show significant differences in detail compared with those from the modified BPP model; the peak heights and positions do not match and the relaxation curves in the rotating frame have a different shape. This indicates that the modified BPP procedure is not a particularly accurate method of modelling the relaxation rates in disordered systems.

The energy distribution used by Markert *et al.* used a width of $\sigma_1 = 0.065$ eV for the Gaussian part of the distribution and a width of $\sigma_2 = 0.04$ eV for the Lorentzian part. It is of interest to examine the sensitivity of the results to the choice of these widths since

the effect of increasing the level of disorder in a system has been noted to cause increased broadening of the relaxation curves and shifting of the peak positions (Adnani, Havill and Titman, 1994). By using a Gaussian distribution of width $\sigma = 0.01, 0.03, 0.05$ and 0.07 for saddle point energy disorder, the relaxation rates for a single frequency in the fixed frame of reference were found to be as shown in figure 4.4. These results are for diffusion between the sites of a single cube. Similar behaviour was observed for systems with larger numbers of sites.

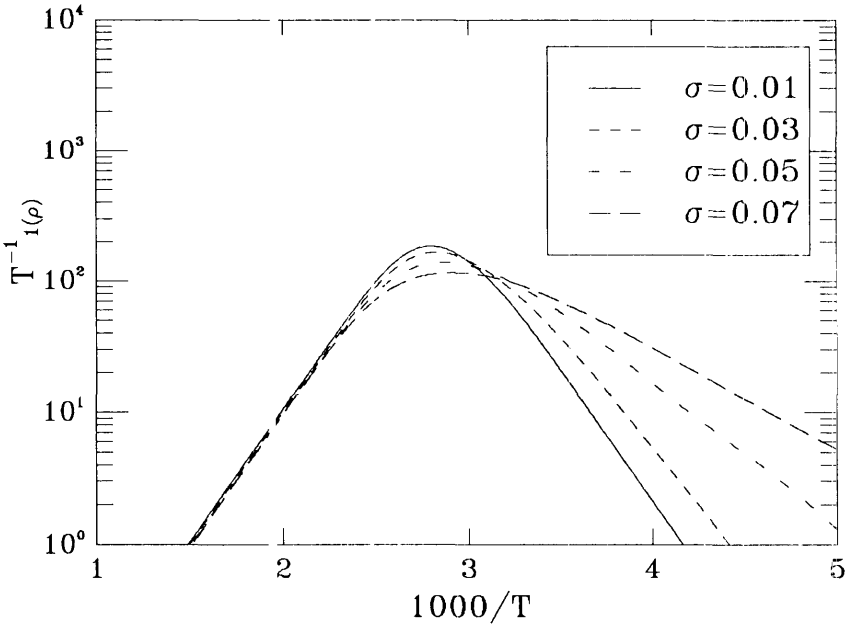

Figure 4.4: Calculated relaxation rates R_1 for four Gaussian widths

As can be seen, as the width of the distribution is increased the relaxation curves become more asymmetrical, and the peak positions are lowered and moved towards lower temperatures. For small values of $\omega\tau$, which corresponds to high temperatures, the behaviour of the curves is virtually identical. As the temperature decreases the curves begin to show different behaviour in line with a slower approach to the large $\omega\tau$ limit. The behaviour of the positions and heights can be more clearly seen in figure 4.5. A width of $\sigma = 0$ corresponds to the ordered crystalline system.

The variation in peak height and position is not very great when going from an ordered system to one with a Gaussian width of $\sigma = 0.01$, but as the distribution becomes wider

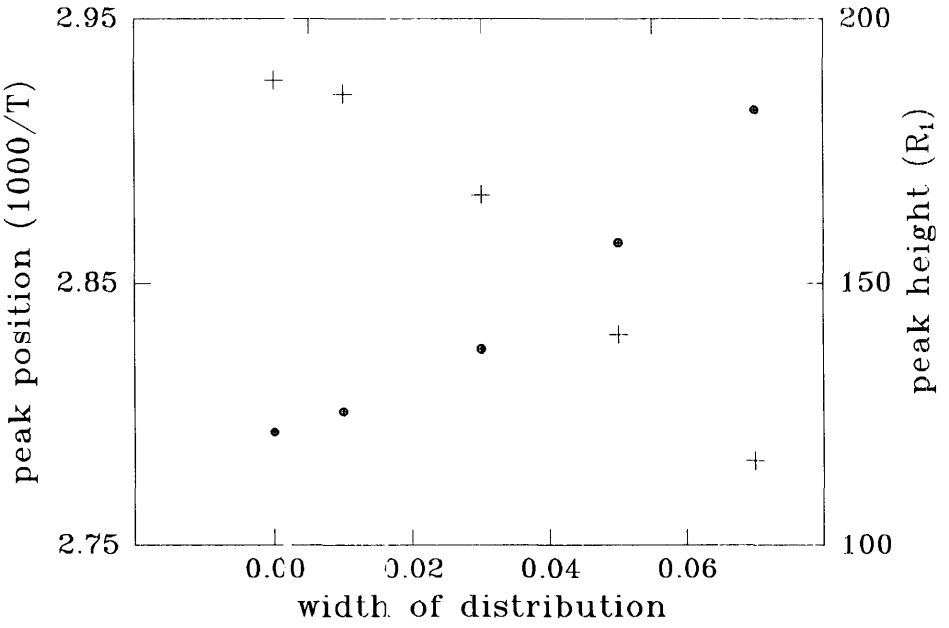

Figure 4.5: Position of peak heights (crosses) and positions (dots) as a function of the width of the Gaussian distribution.

the change is more rapid. The change is not quite linear, with the variations in peak positions curving slightly upwards. The degree of asymmetry in the asymmetric slopes is quite sensitive to the choice of σ which suggests that the observed asymmetry could yield reasonably accurate values of the degree of disorder.

For an ordered system it is possible to generate a set of universal curves for the relaxation for a particular value of $\omega\tau$ such that changing $\omega\tau$ only results in a rescaling of the curves. This is possible because there is only a single τ for the whole system. In a disordered system there is a spread of τ values, so it is no longer possible to generate a single set of universal curves. In this section the choice of variables corresponded to specific numerical values for a particular system. The next section considers the general question of how the relaxation rates depend on particular variables and how theoretical results can be presented.

4.3 Variation of Parameters in a Disordered System

As has been noted in §3.5 an ordered system may be characterised by a single independent parameter $\omega\tau$, defined as

$$\omega\tau = \omega\tau_0 \exp(E_a/kT). \tag{4.1}$$

When relaxation rates are plotted as $\ln R$ versus $\ln(\omega\tau)$, which is equivalent to a plot of $\ln R$ versus $1/T$, results for different experimental frequencies correspond to a scaling of the relaxation curves, giving no new information about the relaxation. Such a set of curves is shown in figure 4.6. The peak of the relaxation curves for the laboratory frame is found at $\omega\tau = C$, where C is of the order of unity, and the relaxation curves at any frequency may be found by a simple scaling of the known set of curves.

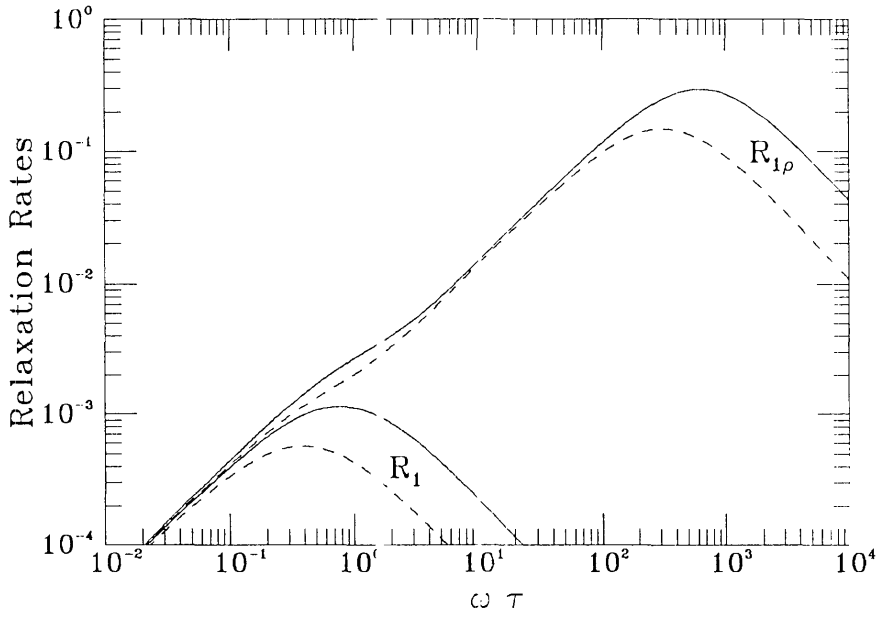

Figure 4.6: Relaxation rates R_1 and $R_{1\rho}$ (arbitrary units) as a function of $\omega\tau$ for the simple cubic lattice and for two different resonant frequencies ω_0 (solid lines) and $2\omega_0$ (broken lines).

For an ordered system the product of τ_0 and $\exp(E_a/kT)$ determines the overall rate at which diffusion proceeds because it is the same at all sites and therefore the single variable

$\omega\tau$ is sufficient to specify the dependence of relaxation on both τ_0 and temperature. There is no such single parameter for disordered systems, as there is no single activation energy E_a and so τ varies from site to site. In practice τ could also vary between sites because of variations in τ_0 but this has not been included in this theory.

One way of presenting the results for disordered systems was described in §3.5. Defining $\omega\tau_a$ such that

$$\omega\tau_a = \omega\tau_0 \exp\left(\frac{E_b - E_s}{kT}\right) \tag{4.5}$$

where E_s and E_b are the average energies of the site and saddle point distributions respectively, the results of relaxation calculations can be presented as $\ln R$ versus $\ln(\omega\tau_a)$ plots for various choices of $\omega\tau_0$. Such plots correspond to experimental plots of $\ln R$ versus $1/T$.

To demonstrate the set of relaxation rate curves produced by this method, the relaxation rates were calculated using the small finite system model for two spins on a twelve point lattice arranged as two adjacent cubes. A distribution of saddle point energies only was included as this has been shown previously to cause broadening of the relaxation rates in line with observed results. The distribution used was Gaussian with a width of $\sigma = 0.06$ and a peak energy of $E_p = 0.40$eV. The ratio between ω and the Larmor frequency in the rotating frame ω_0 was kept at $\omega/\omega_0 = 10^2$ in each case and the data generated for values of $\omega\tau_0 = 10^{-4}, 10^{-5}$ and 10^{-6}. The results appear in figure 4.7.

The relaxation curves are asymmetric in each case and depend on the value of $\omega\tau_0$, unlike those for ordered systems. These results show that measurements for different frequencies provide new information and do not simply correspond to translations of the results for a particular frequency as is the case in ordered systems. The value of $\omega\tau_a$ at which the maximum occurs also depends on $\omega\tau_0$. It is not therefore possible to deduce directly the value of τ_a at the temperature at which the maximum occurs from a relation of the form $\omega\tau_a =$ constant at the maximum, as can be done for an ordered system.

The next section will examine some of the properties of the distribution of eigenvalues and coefficients for a disordered system, as compared to an ordered system. The distribution will be used to explain some of the features of the simulated relaxation rates.

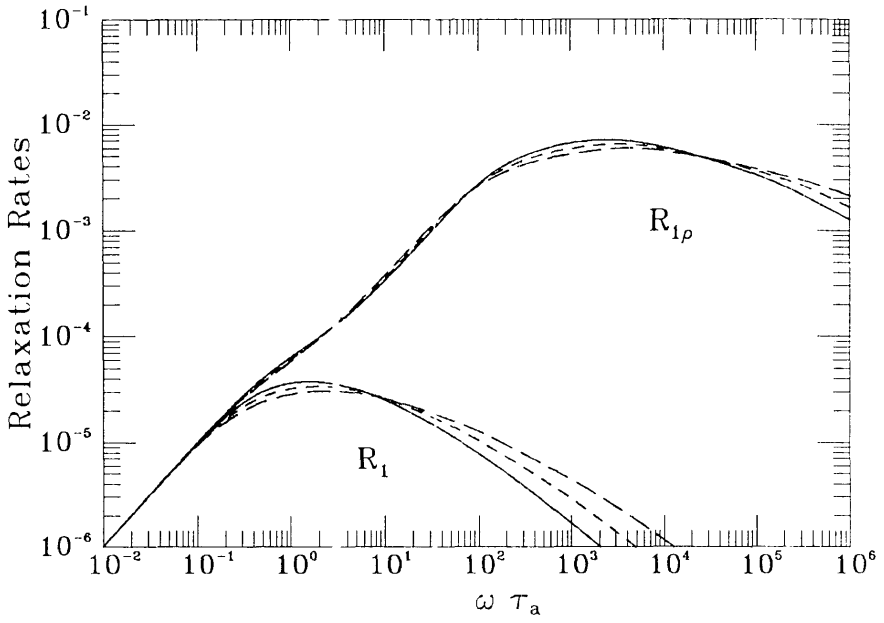

Figure 4.7: Relaxation rates for a Gaussian distribution of saddle point energies with $\sigma = 0.06$ and values of $\omega\tau_0 = 10^{-4}$ (solid curve), 10^{-5} (short dashed curve) and 10^{-6} (long dashed curve).

4.4 Eigenvalues and Coefficients

The correlation functions and spectral density functions for disordered systems may also be written as a linear combination of exponentials and Lorentzians respectively, involving the eigenvalues and coefficients in a similar manner to that for ordered systems, as was shown in §3.4. The form of the distribution of the eigenvalues and coefficients, however, is rather different to that for ordered systems. The presence of disorder, even at a single site or saddle point, is sufficient to remove any degeneracy from the calculated eigenvalues. While it is possible in principle for a spread of jump rates to cause degeneracy to be found in the eigenvalues this was not observed in the simulations. The lack of degeneracy means the solution to equation (3.18) was automatically valid, leading to a spectral density function that was a linear combination of exponentials without having to consider the method of undetermined coefficients.

The inclusion of disorder resulted in a different set of eigenvalues and coefficients for each temperature and random set of site or saddle point energies allocated. The disorder

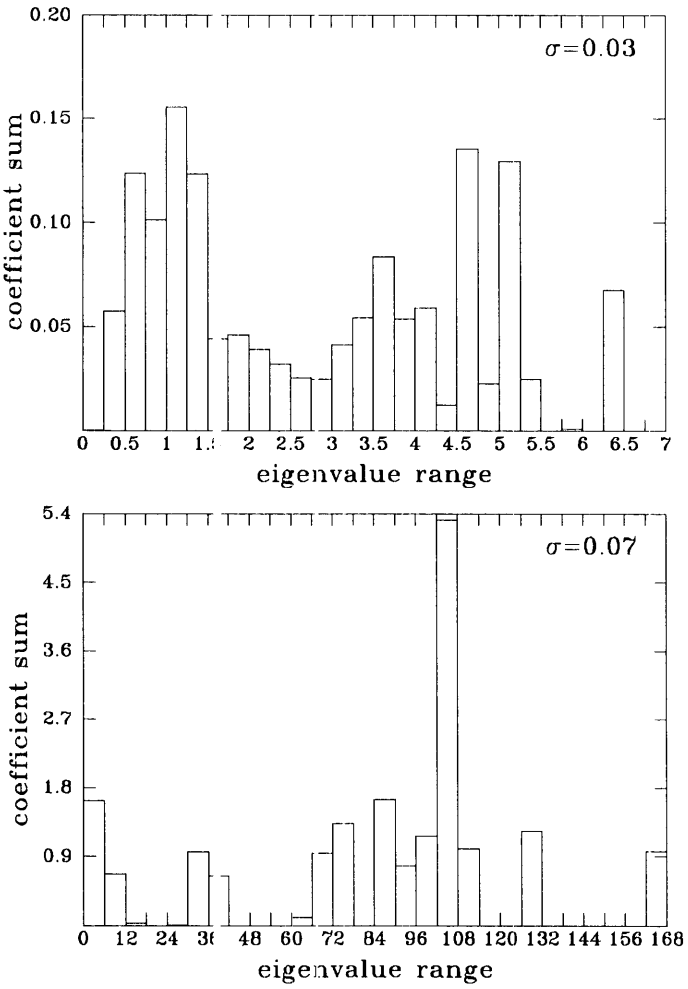

Figure 4.8: Histogram of eigenvalues and coefficients for a 4 cube disordered system, $\sigma = 0.03$ and $\sigma = 0.07$.

was included by choosing a random set of site or saddle point energies from a particular weighted distribution of energy values. The width of the distribution and the peak, or most probable energy value, position could be varied to examine the effect of such changes on the relaxation rates. A typical set of eigenvalues and coefficients for a four cube model with a Gaussian distribution of saddle point energies of width $\sigma = 0.03$ and $\sigma = 0.07$ appears in figure 4.8.

In general there tends to be a wider selection of eigenvalues than is evident in the ordered case. As can be seen the distribution of eigenvalues is much wider for the $\sigma = 0.07$ case than for the $\sigma = 0.03$ case. The magnitudes of the coefficient summations $\sum_i a_i$ for the

ranges of eigenvalues specified in figure 4.8 for the more disordered system are also greater than those of the less disordered system.

Some details of the behaviour of the relaxation rates can be found by examining the histograms in the limit of large and small values of $\omega\tau_a$. The spectral density functions behave as

$$J(\omega\tau_a) = \sum_i a_i \frac{2\lambda_i}{\lambda_i^2 + (\omega\tau_a)^2}. \tag{4.6}$$

where $\omega\tau_a$ is defined as in §4.3. For small values of $\omega\tau_a$ such that $\omega\tau_a \ll \lambda_i$ for all i, this can be simplified to

$$J(\omega\tau_a) = \sum_i \frac{2a_i}{\lambda_i}. \tag{4.7}$$

In this small $\omega\tau_a$ limit the summation terms will become negligible when $\lambda_i \gg a_i$. Examination of this ratio for the $\sigma = 0.03$ and $\sigma = 0.07$ systems shows that the behaviour of the two is very similar. Both show large peaks in the coefficient sum for small eigenvalues (zero to six for $\sigma = 0.07$, zero to two for $\sigma = 0.03$), and negligible values otherwise. This indicates that the behaviour of the relaxation rates for the two distributions will be similar for small values of $\omega\tau$.

For large values of $\omega\tau_a$ such that $\omega\tau \gg \lambda_i$ for all i, equation (4.6) simplifies to

$$\begin{aligned} J(\omega\tau_a) &= 2\sum_i \frac{a_i}{(\omega\tau_a)^2} \\ &= \frac{2}{(\omega\tau_a)^2} \sum_i a_i. \end{aligned} \tag{4.8}$$

As can be seen from the histogram for $\sigma = 0.03$ the condition that $\omega\tau_a \gg \lambda_i$ is satisfied for $\omega\tau_a > 10$ whereas in the $\sigma = 0.07$ case this is not satisfied until $\omega\tau_a > 170$. Also the summation term in the above equation will be different for different energy distributions. For the $\sigma = 0.03$ distribution the summation over the coefficients has a value of 1.457, while for the $\sigma = 0.07$ distribution the summation value is 18.458. The conclusion from both of these is that the relaxation curves will behave differently as the width of the energy distribution is increased. This can been verified by examining figure 4.4 which shows the relaxation rates for four Gaussian distributions of jump rates with different widths. For

small values of $\omega\tau_0$, or high temperatures, the four curves are very similar. For large $\omega\tau_0$ or low temperatures the behaviour changes as the width of the distribution changes.

The next section will detail a method of using the eigenvalue and coefficient distribution for an ordered system to model a disordered one.

4.5 Analytical Approximation

The exact analysis outlined above can be time consuming as several runs for different energy distributions need to be performed to achieve good results for a disordered system. It would be useful to have a simple method to achieve the results. The following is an attempt to develop such a scheme. It is based on combining the results for an ordered system with the distribution of activation energies more directly, analogously to the modified BPP model in §4.2.

The autocorrelation function for the ordered system was defined as a sum of terms, and for an infinite system becomes an integral:

$$G_{ord}(t) = \int_0^\infty A_{ord}(\lambda) \exp(-\lambda w_0 t) d\lambda \tag{4.9}$$

where t is the actual (dimensional) time, λ is dimensionless and corresponds to the eigenvalues of the ordered system, and w_0 is the thermally activated hopping rate given by $w_0 = (1/\tau_0)\exp(-E/kT)$, with the dimensions of $1/t$. $A_{ord}(\lambda)$ is the weighting of each eigenvalue. An attempt was made to fit the function $A_{ord}(\lambda)$ by

$$A_{ord}(\lambda) = a\lambda^n \exp(-\beta\lambda^m). \tag{4.10}$$

The variables n, m, and β were used to fit the form of the curve, with a being a normalisation constant. This curve was fitted to the distribution of eigenvalues and coefficients for two spins diffusing on a twelve cube (or 36 site) simple cubic lattice. This structure was chosen because the shape of the distribution was regular enough to be modelled by a fitted curve.

To reduce the number of independent variables it was decided to match the peak in the histogram with the peak in the fitted curve. Differentiating equation (4.10) and setting $\lambda = 0.6$ as the peak gives $n = \beta m\ 0.6)^m$. Values of m and β were varied to fit the curve and the values $\beta = 1.5$ and $m = 3.2$ obtained. The fit is shown in figure 4.9. The spectral density functions calculated with this function using equation (4.9) agreed well with those

calculated using equation (4.6) with the eigenvalues and coefficients for the 36 site system, as can be seen in figure 4.10.

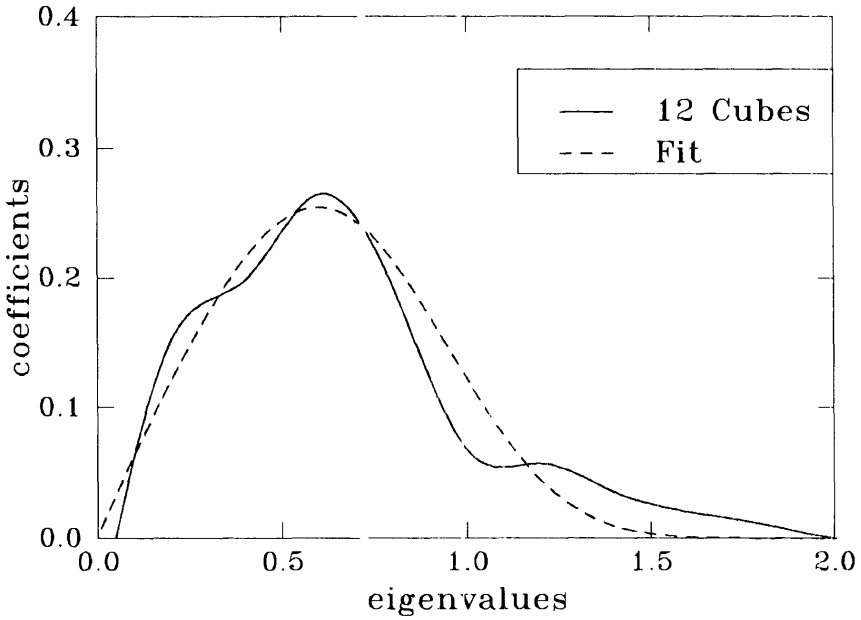

Figure 4.9: Comparison of histogram of eigenvalues and coefficients and fitted curve.

The next step was to extend this model to include disorder. The attempt used was to integrate equation (4.9) over the distribution of jump rates as a function of w, given by $P(w)$, as

$$G(t) = \int_0^\infty P(w) \int_0^\infty A_{ord}(\lambda) \exp(-\lambda \omega t) d\lambda dw \tag{4.11}$$

where w has the dimensions of a rate, and t is actual time. The distribution function $P(w)$ may be calculated in the following way. If there is a normalised distribution of energies given by, for example, a Gaussian function

$$P_1(E) = \frac{1}{\sigma\sqrt{2\pi}} \exp(-(E - E_0)^2/2\sigma^2) \tag{4.12}$$

then each value of E obtained from this distribution corresponds to a jump rate w given by $w = A\exp(-E/kT)$. The probability function $P_1(E)$ needs to be expressed in terms of the distribution function $P(w)$ for the rate w. Since the probability function is normalised,

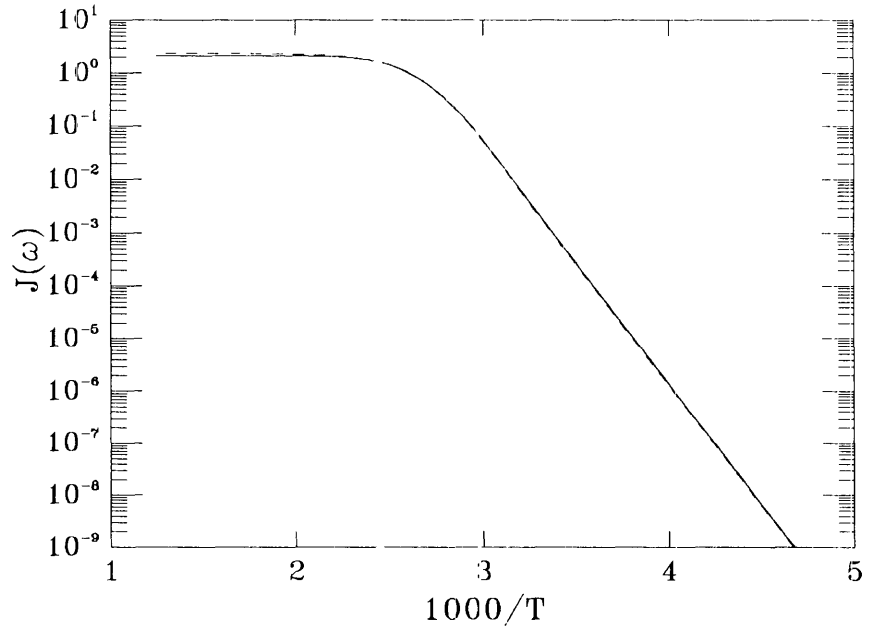

Figure 4.10: Spectral density function for 12 cube system (solid line) and fitted curve (dashed lines).

$$\int_{-\infty}^{\infty} P_1(E)dE = 1. \tag{4.13}$$

Changing the variable by using $w = A\exp(-E/kT)$ yields

$$\int_0^{\infty} P_1(E(w))\frac{dE}{dw}dw = 1 \tag{4.14}$$

i.e.

$$\int_0^{\infty} P(w)dw = 1 \tag{4.15}$$

where $P(w) = P_1(E(w))\frac{dE}{dw}$. The correlation function $G(t)$ can then be calculated.

It is more appropriate to plot the correlation functions and spectral density functions in terms of the dimensionless parameter t'. To achieve this define $t' = \overline{w}t$, where

$$\overline{w} = A\exp(-\langle E\rangle/kT). \tag{4.16}$$

Then the jump rate w can be written as

$$\begin{aligned} w &= A\exp(-E/kT) \\ &= A\exp(-\langle E\rangle/kT)\times\exp(-(E-\langle E\rangle)/kT) \\ &= \overline{w}\exp(-(E-\langle E\rangle)/kT). \end{aligned} \tag{4.17}$$

Substituting this into equation (4.11) gives

$$\begin{aligned} G(t') &= \int_0^\infty P(w)\int_0^\infty A_{ord}(\lambda)\exp(-\lambda w t'/\overline{w})d\lambda dw \\ &= \overline{w}\int_0^\infty p(\overline{w}w')\int_0^\infty A_{ord}(\lambda)\exp(-\lambda w' t')d\lambda dw' \end{aligned} \tag{4.18}$$

where $w' = w/\overline{w}$. So by using equations (4.12) and (4.18) the disordered system may be modelled.

The system modelled was one of saddle point energy disorder, with a Gaussian distribution of energy with width $\sigma = 0.04$ and a peak energy of 0.40eV. The relaxation curves generated by the function in equation (4.18) and a comparison with the exact theory appears in figure 4.11.

The curves have a similar form although there are significant differences. The modelled curves for the rotating frame (upper curves) are broader than for the exact system, and both modelled curves are below those of the exact curves. It is possible that by varying the parameters of the fitted curve that a better fit could be obtained.

Although this method did not reproduce the more accurate results of the small system model particularly well, some functional procedure along these lines would be useful.

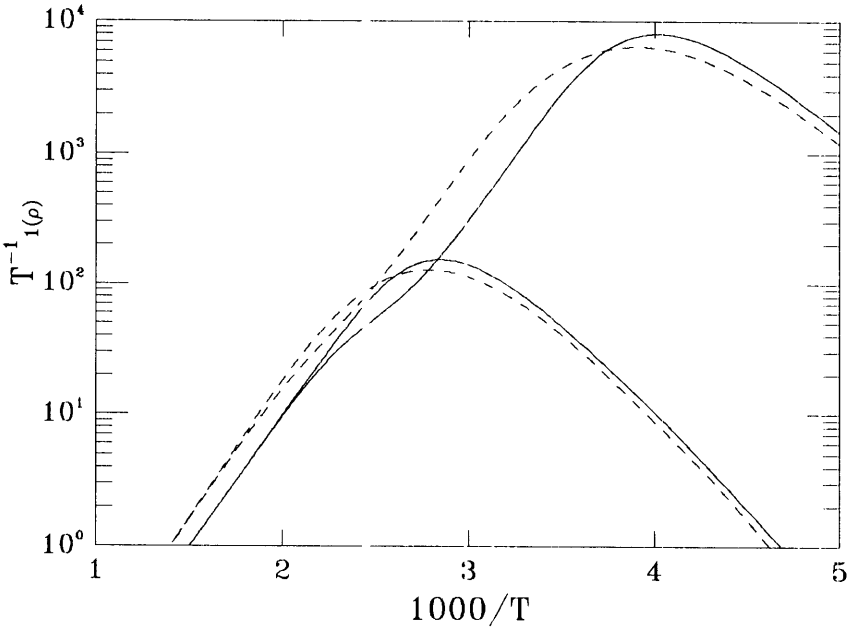

Figure 4.11: Comparison of exact (solid lines) and model function (dashed lines) for relaxation on a single cube.

Chapter 5

Conclusion

Nuclear spin relaxation of spins due to diffusion through a disordered system is quite complex and a large amount of work has gone into attempting to understand the processes involved. Previous work has involved Monte Carlo simulations of the diffusion process to calculate the spectral density functions or fitting curves to the relaxation data. The curve fitting usually involves fitting a distribution of activation energies to a BPP-like expression. While these have given some insight into disordered systems, they do have their drawbacks as was outlined in Chapter 2. For Monte Carlo systems the computing time can be very long, slowly diffusing spins can introduce rounding errors into the calculation of the correlation rates, and numerical Fourier transforms can introduce further errors. Curve fitting, while able to fit the experimental data reasonably well, gives no insight into the processes that effect the diffusion and the fitting quality can degrade at lower spin concentrations (McDowell, 1993). It is questionable whether fitting a distribution of activation energies to a BPP-type expression is a valid method for examining the relaxation rates.

The purpose of this thesis was to determine whether or not the spectral density functions for a disordered system could be modelled accurately using the exact analysis for a low concentration of spins on a small, finite system. Chapter 3 outlined the theory behind the calculation of the spectral density functions which was based on the matrix form of the rate equation

$$\frac{d\mathbf{p}}{dt} = -\mathbf{W}\mathbf{p}. \tag{5.1}$$

The matrix $\mathbf{W}$ was calculated from the probability of a pair of spins moving from one orientation, or state, to another in a jump of either of the two spins. The matrix $\mathbf{W}$ is

singular, meaning that the solutions to equation (5.1) will not be linearly independent. By reducing the matrix $\mathbf{W}$ to $\mathbf{W}'$ an independent set of $n-1$ solutions could be generated, with the n^{th} solution calculated from the others. It was found that despite the ordered system producing a $\mathbf{W}'$ matrix with degenerate eigenvalues, a consistent solution to equation (5.1), which gives the time dependence of the spectral density functions, could be found that was a linear combination of exponentials. This theory is exact only in the low concentration limit, which in this case was two spins on the lattice structure. A disordered system is very complex, so some assumptions on the system were made to simplify the modelling procedure. A simple cubic lattice structure was assumed, rather than a system with different nearest neighbour atomic spacings. The energy disorder on the system was modelled with either site or saddle point energy disorder. These were simplifications of a real system which would involve structural disorder as well as site and saddle point energy disorder, but allowed the effects of the two classes of energy disorder on the spectral density functions to be examined. Structural disorder could be readily included in the model if so desired. It was further assumed that in the definition of the mean time between jumps that the prefactor τ_0 was constant throughout the sample.

The theory was initially applied to modelling an ordered system to check the validity of the model, as the ordered system is well understood and accurate analytic forms for the diffusion in ordered systems exist. The model used was two spins diffusing on an ordered simple cubic lattice consisting of eight lattice sites. With appropriate normalisation it was found that the small, finite system model was a good approximation to the infinite simple cubic system for values of $\omega\tau \gtrsim 1$. In comparison, the BPP model (Bloembergen, Purcell and Pound, 1948) was a poor fit for all values of $\omega\tau$, as expected. The small, finite system model was a poor fit for values of $\omega\tau$ less than one as this corresponds to the high temperature, or long range diffusion, region of the NMR experiment. A small system model cannot be expected to model this region accurately, and this is one of the limitations of the model. A larger lattice size could be used, however the computing time required soon becomes prohibitive. The region in which the model is accurate corresponds to a range of values of $\omega\tau$ from the peak at $\omega\tau \gtrsim 1$ out to lower temperatures, that is, large values of $\omega\tau$.

As modelling a small system exactly was working well for an ordered system the next step was to include disorder in the model. This complicated the calculations as there was no longer a single jump rate for the entire sample but a spread of jump rates from site to site and from jump direction to jump direction. Chapter 4 detailed this application

of disorder to the system. The simulations for a disordered system were compared to the experimental and curve fitting work of Markert *et al.* (1987). It was found that by simulating the diffusion of two spins on a single cube with disorder in the saddle points that similar behaviour to experimental results could be obtained. Saddle point energy disorder lead to the relaxation curves being asymmetrical about the peaks, with the peak heights lowered and the peak positions shifted. Site energy disorder did not cause the relaxation curves to become asymmetrical. To compare the theoretical results of Markert *et al.* to the small system model the energy distribution $G(E_a)$ used in fitting the curve to the experimental results was used to allocate saddle point energy disorder to the model. It was found that the two sets of curves did not agree very well. From this it can be concluded that the modified BPP model, as used by Markert *et al.* does not model the spectral density functions accurately.

Richards and Shinar (1987) had found that site energy disorder caused asymmetry in the relaxation rate curves for disordered systems, rather than saddle point energy disorder. This inconsistency can be explained from the manner in which Richards *et al.* set up their Monte Carlo simulations. They seeded their lattice randomly with spins, allowed them to diffuse and then calculated the correlation functions. This did not allow the system to achieve thermal equilibrium before the simulations were run. Other Monte Carlo simulations, such as those performed by McDowell (1993), began with the system at thermal equilibrium and found that saddle point energy disorder had the greatest effect on the relaxation rate curves.

The method of modelling the spectral density functions by the use of a small, finite system accurately has been shown to be valid in the limit of low concentrations and reasonably short times. For longer times, when long-range diffusion is the dominant feature of the system this model is no longer applicable. By combining this theory with Monte Carlo analysis, which is useful for long time analysis but fails when considering the motion of slow spins, a better picture of the spectral density functions may be developed. The concentration effects can, in theory, be examined, by the use of the mean field theory to simulate the inclusion of more spins in the lattice. By replacing the equilibrium distribution of spins $P_{eq}(\boldsymbol{r}_o)$ by a constant the effect of a high concentration of spins can be simulated. This corresponds to a situation where most of the deep potential wells have been filled, leaving shallower barriers over which the remaining spins can diffuse. The relaxation rates for such a model with site energy disorder were asymmetric, leading to the conclusion that the knowledge of the equilibrium conditions for a system can be important when trying to

understand the processes involved.

In conclusion, the method of analysing small finite systems has been shown to be an effective alternate approach to understanding nuclear spin relaxation in disordered systems which has a firm theoretical basis and is relatively straightforward to apply. This method should prove useful in further work aimed at interpreting nuclear spin relaxation data in disordered systems.

Bibliography

[1] A. Abragam. *Principles of Nuclear Magnetism*. Oxford University Press, Oxford, 1961.

[2] N. Adnani. Hydrogen in amorphous early-late transition metal alloys. *Solid State Communications.*, 90(9):607–611, 199–.

[3] N. Adnani, R.L. Havill, and J M. Titman. Nuclear magnetic relaxation in disordered solids: a Monte Carlo study of metal-hydrogen systems. *J. Phys.: Condens. Matter.* 6:2999–3012, 1994.

[4] A.R. Allnatt and A.B. Lidiard. *Atomic Transport in Solids*. Cambridge University Press, Cambridge, 1993.

[5] W.A. Barton and C.A. Sholl. Nuclear spin relaxation by translational diffusion in solids: V. Reciprocal-space formalism and mean-field theory. *J. Phys. C: Solid State Phys.*, 13:2579–2594, 1980.

[6] N. Bloembergen, E.M. Purcell, and R.V. Pound. Relaxation effects in nuclear magnetic resonance absorption. *Physical Review*, 73(7):679–712, 1948.

[7] R.C. Bowman Jr., A. Attalla, A.J. Maeland, and W.L. Johnson. Hydrogen mobility in crystalline and amorphous Zr_2PdH_x. *Solid State Communications*, 47(10):779–782, 1983.

[8] R.C. Bowman Jr., M.J. Rosker, and W.L. Johnson. A study of the properties and NMR spectra of amorphous and crystalline Zr-Pd hydrides. *J. Non-Cryst. Solids*, 53:105–122, 1982.

[9] L.D. Bustard. Correlated atomic diffusion and its effect on NMR spin-lattice relaxation rates. *Physical Review B*, 22(1):1–11, 1980.

[10] M.A. Crouch, R.L. Havill, and Titman J.M. Nuclear magnetic relaxation and diffusion of hydrogen in an amorphous Ni-Ti alloy. *J. Phys. F: Met. Phys.*, 16:99–108, 1985.

[11] D.J. De Bruin and G.E. Murch. Diffusion correlation effects in non-stoichiometric solids. *Philos. Mag*, 27:1475–1488, 1973.

[12] D.A. Faux, D.K. Ross, and C.A. Sholl. Nuclear spin relaxation by translational diffusion in solids: X. Monte Carlo calculation for the simple hopping model. *J. Phys. C: Solid State Phys.*, 19:4115–4133, 1986.

[13] P.A. Fedders and O.F. Sankey. Correlation functions for simple hopping in a simple cubic lattice. *Physical Review B*, 18(11):5938–5947, 1978.

[14] E. Fukushima and S.B.W. Roeder. *Experimental Pulse NMR: A Nuts and Bolts Approach*. Addison-Wesley Publishing Company, Inc., Reading, Massachusetts, 1981.

[15] J.H. Harris, W.A. Curtin, and M.A. Tenhover. Universal features of hydrogen absoption in amorphous transition-metal alloys. *Physical Review B*, 36(11):5784–5797, 1987.

[16] S. Havlin and B. Avraham. Diffusion in disordered media. *Adv. Phys*, 36(6):695–798, 1987.

[17] S.W. Kelly. *Nuclear Spin Relaxation Due To Quadrupolar Interactions*. PhD thesis, Physics, U.N.E., January 1991.

[18] R. Kirchheim. Solubility, diffusivity and trapping of hydrogen in dilute alloys, deformed and amorphous metals II. *Acta Metall.*, 30(6):1069–1078, 1982.

[19] G. Majer, W. Renz, and R.G. Barnes. The mechanism of hydrogen diffusion in zirconium dihydrides. *J. Phys.: Condens. Matter*, 6:2935–2942, 1994.

[20] J.T. Markert, E.J. Cotts, and R.M. Cotts. Hydrogen diffusion in the metallic glass a-$Zr_3RhH_{3.5}$. *Phys Rev B*, 37(11):6446–6452, 1988.

[21] A.F. McDowell. *Application of NMR to the Study of Motion in Amorphous Nickel-Zirconium Hydride ($Ni_{0.33}Zr_{0.67}H_x$)*. PhD thesis, Cornell University, January 1993.

[22] A.F. McDowell and R.M. Cotts. Hydrogen concentration dependence in the ^{1}H spin-lattice relaxation due to motion in amorphous $Ni_{0.33}Zr_{0.76}H_x$. *Solid State Communications*, 94(7):529–532, 1995.

[23] P.M. Richards and J. Shinar. Effect of distribution of hopping rates on proton NMR in disordered systems. *J. Phys. F: Met. Phys.*, 17:1659–1669, 1987.

[24] C.A. Sholl. Nuclear spin relaxation by translational diffusion in solids. *J. Phys. C: Solid State Phys*, 7:3378–3386, 1974.

[25] C.A. Sholl. Nuclear spin relaxation by translational diffusion in solids: II. Diffusion in BCC and SC lattices. *J. Phys C: Solid State Phys*, 8:1737–1741, 1975.

[26] C.A. Sholl. Nuclear spin relaxation by translational diffusion in solids: XII. An analytical approximation. *J. Phys. C: Solid State Phys.*, 21:319–324, 1988.

[27] C.A. Sholl. Nuclear spin relaxation and diffusion. *Defect and Diffusion Forum*, 95-98:91–106, 1993.

[28] A.C. Switendick. Band structure for metal hydrogen systems. *Z. Phys. Chem*, 117:89–112, 1979.

[29] H.C. Torrey. Nuclear spin relaxation by translational diffusion. *Physical Review*, 92(4):962–969, 1953.

[30] R.E. Walastedt, R. Dupree, J.P. Remeika, and A. Rodriguez. ^{23}Na nuclear relaxation in Na β-alumina: Barrier-height distributions and the diffusion process. *Physical Review B*, 15(7):3442–3453, 1977.

[31] D. Wolf. Determination of self-diffusion mechanisms from high-field nuclear-spin-relaxation experiments. *Physical Review B*, 10(7):2710–2723, 1974.